Modeling Spectral Dissipation in the Evolution of Wind Waves. Part I: Assessment of Existing Model Performance

M. L. BANNER

School of Mathematics, The University of New South Wales, Sydney, New South Wales, Australia

I. R. YOUNG

Department of Civil and Maritime Engineering, University College, University of New South Wales, Canberra, Australian Capital Territory, Australia

(Manuscript received 6 August 1992, in final form 11 November 1993)

ABSTRACT

This study examines the performance of a state-of-the-art spectral wind wave model that uses a full solution to the nonlinear interaction source term. The situation investigated here is fetch-limited wind wave evolution, for which a significant observational database exists. The authors consider both the evolutionary characteristics such as the predicted development of wave energy and peak wave frequency with fetch, as well as the predicted local features of the directional wavenumber spectrum: the spectral shape of the dominant wave direction slice, together with the directional spreading function. In view of the customary practice of constraining the shape of the spectral tail region, this investigation required relaxing the constrained tail assumption. This has led to new insight into the dynamic role of the spectral tail region.

The calculations have focused on the influence of two of the source terms in the spectral evolution (radiative transfer) equation for the energy density spectrum—those due to wind input and to dissipation predominantly through wave breaking. While the form of the wind input source term exerts some influence, the major impact arises from the dissipation source term, for which the authors explore a range of variants of the quasi-linear form proposed by Hasselmann. Due to the nonlinear coupling of spectral components through the wave–wave interaction term, it is only possible to obtain a detailed physical understanding of spectral evolution through such numerical experiments.

The results point to basic shortcomings in the present source terms. These lead to predicted local spectral properties and fetch evolution characteristics that differ significantly from the available observations. It is concluded that further refinement of the dissipation source term is required to improve modeling capabilities for wind sea evolution.

1. Introduction

Reliable prediction of sea state for a prescribed wind field has been a long-standing oceanographic goal with very significant scientific, engineering, and economic benefits. While earlier wind wave generation models focused on the behavior of the significant wave height, more recent models have pursued the prediction of the full directional wave spectrum, based on the numerical solution of the radiative transfer equation. Forms for this general evolution equation appropriate to simplified situations such as homogeneous wind and wave fields with fetch-limited or duration-limited conditions, have been investigated quite extensively for various formulations of the driving (source) terms due to wind input, nonlinear wave–wave interactions, and wave dissipative processes. These source terms have been synthesized from both observational and theoretical results, with the dissipation source term being the least well understood. Additional deep water effects such as refraction by horizontally sheared currents can also be included, but this study is concerned primarily with fetch-limited conditions for which the form of the radiative transfer equation is described in detail in section 3.

Overall, it should be pointed out that operational wave models presently in use (3G-WAM: S. Hasselmann et al. 1988) appear to be successful in predicting significant wave height and peak spectral period over regional areas using observed wind fields. However, as will become apparent in the discussion that follows, certain fundamental aspects and implications of the modeling appear to have been overlooked. These provide a primary focus of this study, in conjunction with a detailed examination of the poorly understood dissipation source term. In this context, it is of interest to comment critically on the present status of these terms.

Corresponding author address: Dr. I. R. Young, Department of Civil and Maritime Engineering, University College, The University of New South Wales, Canberra, ACT 2600, Australia.

Following many years of observational and analytic effort, the wind input source term $S_{in}(\underline{k})$ is known to a reasonable approximation in the wind direction. It is now fairly well established that in the wind direction, $S_{in}(\underline{k})$ may be parameterized using a measure involving a representative wind speed to wave phase speed ratio. There is an ongoing debate as to whether the wind influence at wavenumber $\underline{k}$ is best described by the friction velocity u_*, the 10-m height mean wind speed U_{10}, or the mean wind speed at a height of half a wavelength $U(\lambda/2)$. However, to relate the present findings to previous studies, we have retained u_* as the velocity scale parameterization in the input source function, with a detailed description of this term appearing in section 4. It should be mentioned, however, that in directions oblique to the wind direction, the directional dependence in $S_{in}(\underline{k})$ is not well understood. Both cosine (Komen et al. 1984, henceforth referred to as KHH) and cosine squared (Janssen 1991) forms have been proposed. Walsh et al. (1989) argue that their fetch-limited open ocean data is consistent with a $\cos^{1.6}\theta$ wind effectiveness dependence near the spectral peak. Observational data capable of directly resolving the question over the full gravity wavenumber range is yet to be obtained.

The source term $S_{nl}(\underline{k})$, described more fully in section 3, represents nonlinear wave–wave interactions within the spectrum. The theory for weakly nonlinear interactions for a homogeneous wave field with quasi-Gaussian statistics was developed by K. Hasselmann (1963a,b) and has been described in detail subsequently by several authors (e.g., Webb 1978; Young and Van Vledder 1993). Extensive computations have confirmed that this complex mechanism has a dominant influence on the evolution of the wave spectrum, but $S_{nl}(\underline{k})$ requires a large amount of computational effort for its evaluation as the spectrum evolves. Approximate methods have been devised to reduce this computational effort significantly [e.g., the direct interaction approximation, S. Hasselmann et al. (1985)], which is of particular concern in operational wave modeling applications.

The dissipation of wave energy is believed to be dominated by wave breaking, with additional wave damping associated with wave–turbulence interactions. The impact of these processes is modeled collectively in the term $S_{ds}(\underline{k})$, whose form is presently not known from observations. Theoretically, K. Hasselmann (1974) proposed a model based on the proposition that the wave breaking is weak in the mean and is quasi-linear in the spectral density, whereas Phillips (1985), among others, has argued that $S_{ds}(\underline{k})$ needs to be a nonlinear function of the spectral density. The Hasselmann model has been adopted widely both in model studies and in operational wave models, with apparent success. The K. Hasselmann (1974) formulation, however, only provides insight into the general functional form of $S_{ds}(\underline{k})$, and a wide range of variants is possible within this general form. Their suitability can only be determined through numerical experiments (e.g., KHH).

The focus of the present paper is primarily on the effectiveness of the K. Hasselmann (1974) form of $S_{ds}(\underline{k})$. This has been motivated by the recent availability of data on the shape of the high wavenumber spectrum for gravity waves, together with further observational data on the fetch evolution of wave energy and peak period. In presenting a detailed examination of the behavior of model predictions with these more demanding criteria, this study serves to extend and refine aspects of the key modeling paper by KHH. In a similar manner to their study, we use a full solution to $S_{nl}(\underline{k})$ (Resio and Perrie 1991), which takes into account all nonlinearly interacting wavenumber components in the computational grid. We investigate in detail the performance of the model in fetch-limited growth, examining a range of local spectral properties together with the development of the total wave energy and peak spectral frequency with fetch. These predictions are compared with the available observations, which are reviewed in detail in the following section.

While the variations of $S_{ds}(\underline{k})$ investigated here are necessarily empirical [within the general theoretical framework of Hasselmann (1974)], they provide an intriguing investigation of the physical behavior of a nonlinearly coupled wave model. Due to this nonlinear coupling between spectral components, the sensitivity of the model results to the details of the source term selection is often difficult to predict: this aspect has been largely overlooked in previous investigations.

2. Brief review of relevant observational data

a. *Integrated properties of the spectrum and their evolution*

The now classic JONSWAP wind wave experiment (Hasselmann et al. 1973) provided a valuable dataset on the fetch-limited evolution of the nondirectional frequency spectrum, and offered strong observational support for the major role played by weakly nonlinear wave–wave interactions in the evolution of the spectral peak to lower frequencies and the attendant growth in total wave energy. These growth characteristics have been expressed in nondimensional form and have been used in model calculations (e.g. KHH) to set the proportionality constant level of the dissipation source term $S_{ds}(\underline{k})$. The JONSWAP data was also analyzed to provide a standardized parametric frequency spectrum shape with five shape parameters: these were needed to describe the peak frequency, the peak enhancement factor, its asymmetry, and the spectral level of the tail. The variation of these parameters with dimensionless fetch xg/u_*^2 was also determined. At the

time, a spectral tail exponent of -5 was adopted for the frequency spectrum on the basis of equilibrium spectral ideas advanced by Phillips (1958). Subsequent reanalysis of the JONSWAP dataset by Battjes et al. (1987) showed that statistically an exponent of -4, as first proposed by Toba (1973), was a better approximation to the data.

The very detailed observational study by Donelan et al. (1985, henceforth referred to as DHH) of deep-water wind wave evolution on Lake Ontario provided new insight into the behavior of the frequency spectrum up to three times the peak frequency. Their dataset spanned a particularly wide range of wave age, C_p/U_{10}, where C_p is the phase speed of components at the spectral peak and U_{10} is the wind speed measured at a reference height of 10 m. An array of 14 wave gauges was used to provide relatively high directional resolution for frequencies up to $1.6f_p$, where f_p is the frequency of the spectral peak. Above this value their directional spreading appears to become noisy. The directional spreading characteristics reported by DHH differ substantially from those reported in earlier studies based on pitch–roll buoy data with intrinsically poorer directional resolution (e.g., Mitsuyasu et al. 1975; Hasselmann et al. 1980). The major differences are shown clearly in Fig. 7 of DHH, with the pitch–roll buoy directional distributions showing a much more rapid broadening with increasing distance from the spectral peak.

DHH estimated the effective fetch from the dominant wave direction and the effective wind velocity, $U\cos\theta$, where θ is the angle between the mean wind and dominant wave directions. On this basis, they reported on the evolution of the key spectral parameters as a function of the nondimensional fetch, but these proved to be considerably different from the JONSWAP fetch correlations. Using their aircraftborne surface contour radar, Walsh et al. (1989) reported a case of fetch-limited evolution off the U.S. East Coast that showed closer conformity to the JONSWAP fetch relationship than to the DHH correlation. At very long fetches, reliable data is rare as the requirements of steady state are seldom met. The classic dataset of Pierson and Moskowitz (1964, henceforth referred to as PM) indicates an asymptotic limit to growth.

Figure 1 shows the nondimensional growth rate ($E^* = E_{tot}g^2/u_*^4$ vs $x^* = xg/u_*^2$) and peak frequency development ($f_p^* = u_*f_p/g$ vs $x^* = xg/u_*^2$) for these studies. The original results for all these studies were scaled in terms of the observed wind speed U_{10}, so in order to construct Fig. 1 it was necessary to determine an appropriate drag coefficient C_d and hence u_* for each case. For the JONSWAP dataset the measured value of $C_d = 1.00 \times 10^{-3}$ was used. For each of the other datasets a representative value of U_{10} was selected and the relationship of Wu (1982) used to determine C_d. The values adopted were DHH: $U_{10} \approx 10$ m s^{-1}, $C_d = 1.45 \times 10^{-3}$; Walsh et al.: $U_{10} \approx 12$ m s^{-1}, $C_d = 1.58 \times 10^{-3}$; and PM: $U_{10} \approx 15$ m s^{-1}, $C_d = 1.80 \times 10^{-3}$.

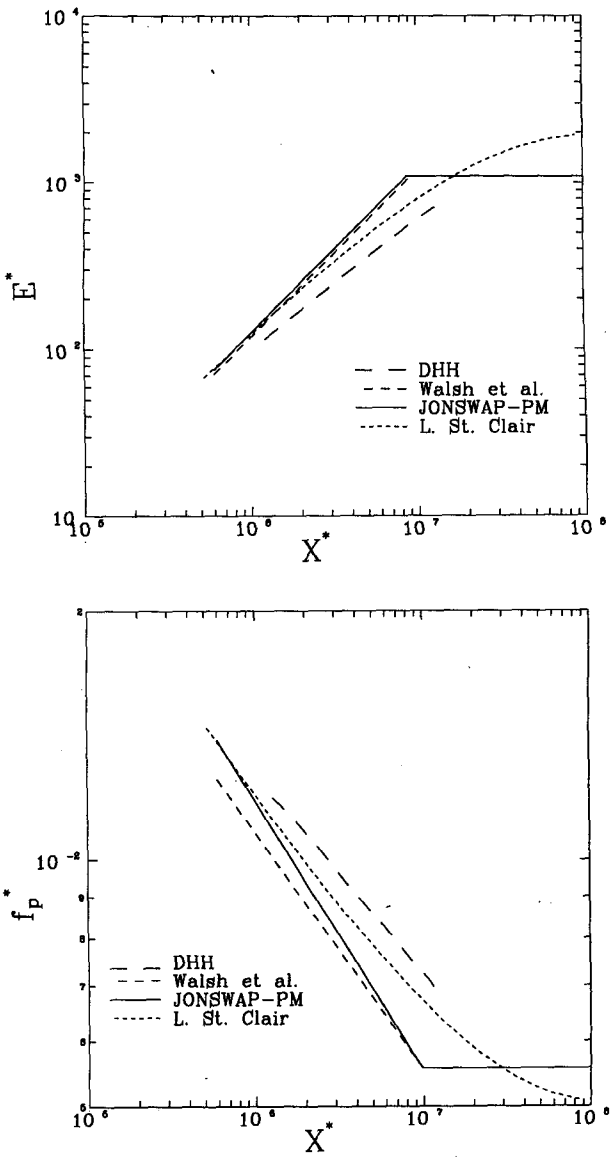

FIG. 1. Development of the nondimensional energy E^* and nondimensional peak frequency f_p^* as a function of nondimensional fetch x^*. Results from the observational data of Donelan et al. (1985); Walsh et al. (1989); the combined JONSWAP (K. Hasselmann et al. 1973) and PM (Pierson and Moskowitz 1964) results; and Donelan et al. (1992) are shown.

It is noted that following the pioneering work of Donelan (1982), recent studies conducted in waters of limited depth (e.g., Geernaert et al. 1987; Smith et al. 1992), have confirmed a sea state influence on the wind stress, with a significant enhancement of C_d reported for very young wind seas. The impact for deep water conditions is not yet known and the Wu (1982) for-

mulation used above includes no sea state dependence. Even if the deep water implications were known, it would require a complete reanalysis of the datasets involved to determine how the deep water growth curves shown in Fig. 1 would be modified. While this is beyond the scope of the present study, the potential impact of including a sea state influence was addressed in this study, as described in section 5.5 below.

The differences between the fetch-limited datasets mentioned above are significant and despite a detailed reexamination of the respective datasets by Kahma and Calkoen (1992), the reasons for such differences are yet to be fully resolved. Further elucidation of this issue is provided by the very recent detailed study of deep water wave evolution with fetch on Lake St. Clair by Donelan et al. (1992). They used a line array of wind/wave measurement towers deployed along the fetch and examined the differential growth between these stations to avoid the usual assumption of homogeneous wind conditions over long fetches. When scaled in terms of U_{10}, their analysis provided fetch relations for the nondimensional wave energy, peak frequency, and wave age close to the JONSWAP relations except that these show a smooth transition to a fully developed state consistent with the PM result. The recent open ocean field results reported by Ebuchi et al. (1992) also conform closely to the Lake St. Clair results. However, when scaled in terms of u_* (assuming $U_{10} \approx 7$ m s^{-1}, $C_d = 1.26 \times 10^{-3}$), the Lake St. Clair results diverge from JONSWAP and yield an asymptotic level greater than the PM result (see Fig. 1). Notwithstanding such difficulties and the unresolved differences between datasets, the basic trends of these datasets provide a useful basis for assessing the model performance in predicting the growth of wave energy and peak frequency evolution with fetch.

b. *Observed wavenumber spectral properties*

From their extensive directional wave gauge array measurements, DHH proposed a form for the directional frequency spectrum near the spectral peak. This includes a spreading functional dependence of the form

$$D(\theta; k) = \operatorname{sech}^2\beta(\theta - \theta_w), \qquad (2.1)$$

where k is wavenumber, θ is the polar direction, and θ_w is the wind direction. DHH found that the primary variation of β was on k/k_p or (f/f_p), where k_p is the wavenumber of the spectral peak (see DHH Fig. 32), with no appreciable dependence on wave age (C_p/U_{10}). For $f/f_p < 1.6$, the DHH spreading function (2.1) using β given by their Eq. (8.4) provides a very useful observational reference for the spreading function close to the spectral peak. This is one of the spectral shape diagnostics used in assessing the model performance in this study. However, to examine the quality of the model predictions at shorter scales than this, it is noted that beyond $f/f_p \approx 1.6$, the DHH data for β become very noisy and a more realistic account of the directional properties of the wind wave spectrum needs to be used.

Based on a synthesis of available wavenumber and frequency spectral observational data, Banner (1990, henceforth referred to as B90) has highlighted the key role of directionality in shaping the frequency spectrum. Banner argued that the DHH proposal that $\beta = 1.24$ for $f/f_p > 1.6$ cannot hold, and that β must continue to decrease with increasing f/f_p. Banner [his Eq. (2.9b)] presents a form for β that transitions from the DHH values below $f/f_p \approx 1.6$ to values consistent with the high gravity wavenumber results reported by Banner et al. (1989). This deduced behavior for β has since been confirmed observationally by M. Donelan (1990, personal communication).

Banner also argues that the limited available wavenumber spectrum data are consistent with a wind direction slice ($\theta = \theta_w$) for the wavenumber spectrum of the form

$$F(k, \theta_w) = 4.5 \times 10^{-5}(U_{10}/C_p)^{0.5}k^{-4} \qquad (2.2)$$

(k is in cycles per meter), for the spectral region corresponding to $1.2 < f/f_p < 3$. This form is also applicable for $f/f_p > 3$, as discussed in 2.3 below. For $1.2 < f/f_p < 3$, B90 has shown that (2.1) and (2.2) with the extended DHH parameterization for β based on Eq. (2.9) in B90 yield a frequency spectral dependence of $f^{-3.7}$. This is entirely consistent with the observed behavior of the frequency spectra shown in DHH Fig. 12, to which DHH have chosen to fit f^{-4}. In any event, this degree of conformity proves suitable for our choice of (2.1) and (2.2) as a representative basis for observed wavenumber spectral behavior near the spectral peak and beyond, as discussed in the following section.

c. *Observed spectral properties toward higher wavenumbers*

Toward shorter scales, the behavior of the tail of the wavenumber spectrum in the ocean has come under recent observational scrutiny with studies by Banner et al. (1989) and M. Banner and I. Jones (1993, personal communication) covering the short gravity range from 5- down to about 0.3-m wavelengths, which embraces the shortest wavelengths (1.85 m) resolved in the present study. The main results for the short gravity range were:

1) The wavenumber spectral slice in the dominant wave direction is close to k^{-4}, with a very weak wind speed dependence [cf. (2.2)].

2) The directional spreading width typical of this short gravity wave regime is broad, consistent with isotropic (circular) *folded* directional wavenumber spectra obtained stereophotogrammetrically. These findings

are consistent with L-band (23 cm) radar backscatter data reported by several investigators, most recently Keller and Plant (1990).

Based on these high wavenumber observations, the relations (2.1) and (2.2) with the spreading factor β modified for higher wavenumbers (corresponding to gravity wave scales with $f/f_p > 3$) were also used by B90 to predict the shape and level of the gravity range tail of the frequency spectrum for $f/f_p > 3$. Close agreement with observed frequency spectra was achieved over a wide range of wave age conditions, after including the influence of Doppler shifting effects. It is noted that while some margin for variation of the dependences in (2.2) is certainly possible, calculations indicate that the wavenumber exponent needs to be close to -4 in order to maintain consistency with observed levels of the mean square slope of the sea surface (e.g., Cox and Munk 1954; Jackson et al. 1992).

The wavenumber spectral dependences embodied in (2.1) and (2.2) for the high wavenumber wind direction slice and directional spreading were used as the basis for assessing the model predictions in the short gravity wavenumber tail region. Comparison with the model predictions was carried out by transforming the above forms using (5.1)–(5.4) below.

The availability of these local observational results for the spreading near the peak and the higher wavenumber spectral behavior extends the basis for assessing wave model performance, particularly the validity of proposed forms for the dissipation source function. This has further relevance in the context of coupling wind and wave models (e.g., Janssen et al. 1989; Janssen 1991). In that application, the short wave scales support a significant fraction of the wave-coherent wind stress, so that unrealistic representation of the short scales is likely to contribute to less reliable wind stress estimates.

3. Description of model

In the absence of currents, the evolution of the wave spectrum can be described by the energy transfer equation (Gelci et al. 1957; K. Hasselmann 1960; Willebrand 1975), which for deep water is

$$\frac{\partial F}{\partial t} + \underline{C_g} \cdot \nabla F = S_{\text{tot}}, \tag{3.1}$$

where $F = F(\underline{k}; \underline{x}, t)$ is the two-dimensional wavenumber spectrum. Equation (3.1) describes the evolution of the spectrum, components of which are advected at their respective group velocity $\underline{C_g}$. The source term S_{tot} represents all processes that transfer energy to or from spectral components. It may be written in the form (K. Hasselmann 1960)

$$S_{\text{tot}} = S_{\text{in}} + S_{\text{nl}} + S_{\text{ds}}, \tag{3.2}$$

where S_{in} represents the atmospheric input from the wind, S_{nl} is the nonlinear interactions between spectral components, and S_{ds} is the dissipation due to white capping and other processes. Here, and in the remainder of this paper, the wavenumber dependence of all source terms is not explicitly shown.

For the case of steady-state fetch-limited growth, (3.1) reduces to

$$C_g \cos\theta \frac{\partial F}{\partial x} = S_{\text{tot}}, \tag{3.3}$$

where x is the distance offshore measured perpendicular to the assumed infinitely long shoreline. Following KHH, (3.3) was solved using a first-order forward difference scheme. The space step Δx was dynamically adjusted so as to maintain numerical stability and accuracy.

a. Details of the computational grid

The directional wavenumber spectrum $F(\underline{k})$ was defined on a polar grid. A total of 37 angular bands were defined in the range $\pm 120°$ of the wind direction, thus yielding a directional resolution of 6.67°. A logarithmic wavenumber spacing consisting of 43 bands spaced according to the relationship $k_n = 1.13k_{n-1}$, with $k_0 = 3.18 \times 10^{-3}$ cpm was adopted. Hence, the highest spectral component resolved by the model was 0.540 cpm (0.92 Hz with a wavelength of 1.85 m). Resio and Perrie (1991) have investigated a number of spectral resolutions and found choices comparable to the one utilized here to be adequate.

b. Source terms

The forms for S_{in} and S_{ds} will be described in detail in the next section. The nonlinear source term, S_{nl}, was evaluated using the technique described by Tracy and Resio (1982) and Resio and Perrie (1991). This technique was favored over the better-known technique of Hasselmann and Hasselmann (1981) as it is slightly more computationally efficient. A number of evaluation tests were performed to ensure the two methods produced comparable results. An exact comparison cannot be performed due to the different computational grid formulations used by the two techniques.

The nonlinear energy transfer represented by S_{nl} involves the interaction of four wavenumbers $\underline{k}_1, \underline{k}_2, \underline{k}_3$, and $\underline{k}_4$, which satisfy certain resonance conditions (Hasselmann 1962). The solution technique of Resio and Perrie (1991) defines the values of $\underline{k}_1$ and $\underline{k}_3$ on the polar grid described above. With a selected combination of $\underline{k}_1$ and $\underline{k}_3$, the values of $\underline{k}_2$ and $\underline{k}_4$ that satisfy the resonance conditions will trace out two "egg-shaped" loci in wavenumber space. The nonlinear energy transfer can be evaluated by integrating around these loci. In keeping with the suggestions of Resio and

Perrie (1991), these loci were discretized with 50 points to perform these line integrations.

Although the values of spectral energy are defined at each of the $\underline{k}_1$, $\underline{k}_3$ points, the $\underline{k}_2$, $\underline{k}_4$ values will generally be at nongrid points and the energy at these points was evaluated using bilinear interpolation within the computational grid defining the $\underline{k}_1$, $\underline{k}_3$ points.

COMPUTATIONAL ASPECTS OF THE HIGH WAVENUMBER REGION

Some of the loci defining the $\underline{k}_2$, $\underline{k}_4$ points extend beyond the high wavenumber cutoff (0.540 cpm). To include these interactions, the energy at such points was evaluated by extending the computational grid with an analytical tail (Hasselmann and Hasselmann 1981), henceforth referred to as the computational tail extension. Sensitivity tests were performed with a number of forms for this tail. Provided the explicit computational grid was extended to relatively high wavenumbers (relative to the wavenumber of the spectral peak), as adopted above, the computational tail extension biased only the last two or three computational points in the explicit grid. A form for this tail with $F(\underline{k}) \propto k^{-3.5}$, which is equivalent to $E(f) \propto f^{-4}$, was finally adopted. The constant of proportionality was set independently for each directional band so that the energy of the first point of the computational tail extension was equal to the last point in the explicit computational grid for that direction.

The S_{nl} computations have been assumed valid for gravity wave components out to 0.540 cpm, and one must question the high wavenumber validity of the Hasselmann (1962) S_{nl} representation. K. Hasselmann (1993, personal communication) indicates there is no rigorous derivation of the limits of the nonlinear expansion method. There are, however, a number of limiting conditions that arise in the derivation of the transfer integral.

(i) One requirement is that the characteristic time scale for the rate of change of the spectrum for any spectral component must be large compared with the wave period. This is satisfied for essentially all waves, even at very high wavenumbers.

(ii) A second requirement, which is appropriate for the peak of the spectrum, is that the characteristic time scale must be large compared with the inverse frequency width of the spectrum. This is always satisfied, even for very narrow spectral forms. This condition has no influence on the high wavenumber validity of S_{nl}.

(iii) Finally, there is the requirement that the conditions at the surface boundary can be linearized using a Taylor series about the mean water level. As the high wavenumber waves are superimposed on the lower wavenumber components of the spectrum, they will be periodically displaced above and below the mean water level. As the wavenumber of these short waves increases or as the amplitude of the longer waves increases, the accuracy of the Taylor series expansion gradually decreases. K. Hasselmann (1993, personal communication) indicates that the limit to validity can be expressed in terms of the ratio of the rms spectral wave height to the short wave wavelength, H_{rms}/L_{short}. The expansion is valid provided H_{rms}/L_{short} is less than O(1). In the present computations H_{rms} reaches a maximum value of 0.3 m and the high wavenumber spectral cutoff corresponds to $L_{short} = 1.85$ m ($k = 0.540$ cpm). Hence, we approach but do not exceed the high wavenumber limit on the validity of S_{nl}. As this limit is not rigorous, an additional run was performed where the high wavenumber limit was truncated at 0.3 cpm (approximately half the standard value used). Although there are minor differences between the runs as one would expect, there were certainly no major changes in spectral development that would lead one to believe that our choice of high wavenumber cutoff invalidated the nonlinear theory.

Another consideration concerns the size of the inhomogeneous terms in the transport equation (Hasselmann 1971; Watson and West 1975) for high wavenumber spectral components. For the calculations reported in this paper, typical Doppler shifting of the high wavenumber spectral components by the lower wavenumber components was, at worst, 0.25 times the intrinsic frequency. In addition, calculations of a typical inhomogeneous term showed a worst case level of less than 10% of the homogeneous S_{nl} contribution. On this basis the homogeneous terms appear to dominate the development of the spectrum in the adopted wavenumber range. Consequently, it has been assumed that the contribution of the inhomogeneous terms can be neglected.

c. Initial conditions

The initial condition selected for all runs consisted of a mean JONSWAP spectrum with a $\cos^2\theta$ directional spread. The peak frequency f_p was varied depending on the wind speed being investigated ($U_{10} = 5$ m s^{-1}, $f_p = 0.5$ Hz; $U_{10} = 10$ m s^{-1}, $f_p = 0.3$ Hz; $U_{10} = 20$ m s^{-1}, $f_p = 0.2$ Hz). Again, a number of sensitivity runs were performed with alternative initial spectral forms. As reported by Komen et al. (1984), model results are very insensitive to the assumed initial spectral form, the spectrum very quickly being shaped to a form consistent with the source terms. The only influence of the initial condition is that it sets the initial total energy for the run. As the specification of f_p is a convenient method to set this initial energy, this parameter was varied for the differing wind speed runs.

4. Scope and aims of computations

The numerical wave model study using the radiative transfer equation by KHH provides the starting point

for this investigation. These authors examined the asymptotic (long fetch) behavior for fetch-limited wind wave growth, corresponding to well-developed seas. Their choice of source terms was as follows:

S_{in}: Snyder et al. (1981) form, converted from U_5 to u_* assuming a wind speed–dependent drag coefficient due to Wu (1982), applicable over the entire spectrum. This form is based on the observed dependence of the variable $(U_5 \cos\theta/C - 1)$, which expresses the relative wind to wave component velocities.

S_{nl}: EXACT-NL form due to Hasselmann and Hasselmann (1981).

S_{ds}: Hasselmann (1974) whitecap pressure pulse model form with $S_{ds} = S_{ds}[k, F(\underline{k})]$, tuned to give the Pierson–Moskowitz (1964) fully developed spectrum equilibrium range level. Specifically, KHH explored the implementation of the form

$$S_{ds}(\underline{k}) = -c\bar{\omega}\left(\frac{\omega}{\bar{\omega}}\right)^{l}\left(\frac{\hat{\alpha}}{\hat{\alpha}_{PM}}\right)^{m} F(\underline{k}) \qquad (4.1)$$

for different values of the exponent l and the level constant c. In (4.1), $\bar{\omega}$ represents the mean spectral frequency $[\bar{\omega} = E_{tot}^{-1} \int \omega F(\underline{k}) d\underline{k}]$ and $\hat{\alpha}$ is a measure of the mean wave slope $(\hat{\alpha} = E_{tot}\bar{\omega}^4/g)$; $\hat{\alpha}_{PM}$ is the theoretical value of $\hat{\alpha}$ for a PM spectrum (KHH). These numerical experiments were necessary since the Hasselmann (1974) theory provides only the general functional form for S_{ds}, many variants being possible within this functional framework.

A key feature of the KHH calculations should be noted: to accelerate the computations, a fixed shape high-frequency spectral tail ("diagnostic tail") of the form $E(f) \propto f^{-5}$ was imposed for frequencies $f > 2.5 f_p$, where f_p is the spectral peak frequency. No explicit computations were performed in this spectral region, the diagnostic tail defining the spectral form. It was stated that the results obtained were insensitive to the details of this high-frequency tail parameterization, as well as to the choice of frequency and directional discretization and the numerical integration scheme used in the computations. What will become apparent from the present study is that the imposition of this fixed spectral tail shape has a very significant influence on the calculations and on the evolution of the spectral peak.

In essence, KHH optimally tuned the coefficient c in S_{ds} [Eq. (4.1)] for different values of the exponent l, under the fixed tail shape approximation. The end result was a two-dimensional frequency spectrum for well-developed seas that approximated "reasonably" the available empirical growth curve data (KHH Figs. 6 and 8) and had a reasonable directional spectral distribution of energy (KHH Fig. 9).

The focus of the present study is on the validity of the Hasselmann form of S_{ds}, in light of recent improvements in our understanding of the wavenumber spectral form both near the spectral peak and at high wavenumbers in the gravity range. Clearly, this necessitated relaxing the constraint of a fixed diagnostic tail shape and embracing higher wavenumber components in the tail of the spectrum, which are more strongly wind forced. Based on the availability of fairly well-established refinements to the input source function for strongly forced wave components (e.g., Plant 1982; Donelan and Pierson 1987), we decided to introduce the composite form for $S_{in}(\underline{k})$ proposed by Yan (1987):

$$S_{in}(\underline{k}) = \left\{\left[0.04\left(\frac{u_*}{C}\right)^2 + 0.00544\,\frac{u_*}{C} + 0.000055\right]\cos\theta - 0.00031\right\}\omega F(\underline{k}). \qquad (4.2)$$

This reduces to the Snyder et al. (1981) form for spectral components with weak wind forcing, and to the Plant (1982) form for the more strongly forced components.

The impact of these two changes was assessed in the context of the KHH model, with the computational experiments documented in Table 1. Having isolated these influences, the free tail computational runs (designated by UT descriptor in Table 1) with the composite form for S_{in} (designated by Y descriptor in Table 1) were then extended to a detailed examination of the effect of varying the parameters in the Hasselmann dissipation source term S_{ds}. Finally, the consequences of assuming a sea state–independent aerodynamic drag coefficient as in the Wu (1982) formulation is assessed by a comparison with a run utilizing the sea state–dependent relationship of Geernaert et al. (1987). All experiments are listed in Table 1, with details of the various wind speeds and dissipation parameters. The results of the suite of computations are described in detail in the following section.

5. Results of the numerical experiments

a. Source term performance diagnostics

Section 5b describes results of the various numerical experiments presented in Table 1, together with comparisons with available observational data. In particular, we focus on four spectral characteristics: (i) total energy and peak frequency development with fetch, (ii) wavenumber spectral slice characteristics (spectral slope and level) in the dominant wave direction, (iii) the full directional wavenumber spectrum, and (iv) the directional spreading distribution. The commonly used one-dimensional or omnidirectional frequency spectrum is a weighted integral of (ii) and (iii). As such, comparisons between observed and model results of one-dimensional frequency spectra are often inconclusive. From such comparisons it is not possible to

TABLE 1. A summary of the atmospheric input, S_{in}, and dissipation, S_{ds}, source terms used for each of the numerical experiments. The relative tail energy parameter ϵ obtained from Eq. (5.5) is also shown where appropriate.

Name	Form of S_{in}	Form of S_{ds}	Comment	ϵ
K10UT	Komen et al.	Komen et al.	Unconstrained tail	2.60
K5UT	Komen et al.	Komen et al.		
K20UT	Komen et al.	Komen et al.		
K10CT	Komen et al.	Komen et al.	Constrained tail	1.68
K5CT	Komen et al.	Komen et al.		
K20CT	Komen et al.	Komen et al.		
Y10UT	Yan	Komen et al.		3.41
K10UTN	Komen et al.	0.1 × Komen et al.		3.77
K10UTL	Komen et al.	0.5 × Komen et al.		3.04
K10UTH	Komen et al.	2.0 × Komen et al.		2.24
Y10UTO3	Yan	$(\omega/\bar{\omega})^3$	$S_{ds} \propto \omega^3$	2.76
Y10UTO4	Yan	$(\omega/\bar{\omega})^4$	$S_{ds} \propto \omega^4$	0.96
K10UTCD	Komen et al.	Komen et al.	Sea state–dependent C_d	2.81

determine whether differences result due to differing energy levels in the wind direction or different directional spreading. In contrast to previous studies, interest is not confined only to the energy-containing region near the spectral peak. However, it has been shown by several authors (e.g., B90) that for frequencies above approximately $3f_p$, the frequency spectrum is distorted by orbital Doppler shifting by waves at the spectral peak. As with all previous models, the numerical model used in this study does not include such effects. For these reasons frequency spectra are not included in the following discussion.

Although examination of the full two-dimensional spectrum is insightful, its two-dimensional nature makes detailed comparisons with observational data cumbersome. For this reason, a number of integral spectral parameters have been adopted as performance diagnostics for comparisons between model results and observations. These diagnostics include

(i) The evolution of the nondimensional energy, E^*, and peak frequency, f_p^*, with nondimensional fetch, x^*.

(ii) The behavior of the wind direction slice of the wavenumber spectrum, $F(k, \theta_w)$, which for wavenumbers significantly above the spectral peak can be represented by a power relationship of the form

$$F(k, \theta_w) = \alpha u_*^{-2(n+4)} g^{(n+4)} k^n, \qquad (5.1)$$

where k has units of cpm. The parameters α and n were determined using a least squares fit to wavenumbers greater than $6.25k_p$ ($2.5f_p$).

(iii) The directional spreading of the spectrum as defined by the wavenumber-dependent directional spreading function, $D(\theta; k)$:

$$F(\underline{k}) = F(k, \theta_w) D(\theta; k). \qquad (5.2)$$

(iv) It will be shown later that, in contrast to most observations, model results do not always indicate that the directional energy maximum is in the wind direction. In such cases, the magnitude of the ratio of the maximum energy in the spectrum to the energy in the wind direction can be represented by the lobe ratio, λ:

$$\lambda(k) = F(k, \theta)_{max}/F(k, \theta_w), \qquad (5.3)$$

where $F(k, \theta)_{max}$ is the maximum value of the directional wavenumber spectrum at wavenumber k. Hence, a value of $\lambda = 1$ indicates a unimodal directional spread.

(v) A further useful parameterization of the directional spreading can be achieved through the definition of a mean spectral width, $\bar{\theta}(k)$, given by

$$\bar{\theta}(k) = \frac{\int_0^{\pi/2} F(k, \theta)\theta d\theta}{\int_0^{\pi/2} F(k, \theta) d\theta}. \qquad (5.4)$$

(vi) It is desirable to know whether a change in a particular source term results in an increase or decrease in the magnitude of the energy level of the spectral tail. Examination of α obtained from (5.1) cannot always provide this information directly, as the energy level also depends on the exponent n. Hence, a further indicator ϵ is introduced, where

$$\epsilon = \frac{F(k = 0.5 \text{ cpm}, \theta_w)}{F(k = 0.5 \text{ cpm}, \theta_w)_{\text{Eq.(2.2)}}}, \qquad (5.5)$$

where both spectra are evaluated at $C_p/u_* = 16$. That is, ϵ is the ratio of the wind direction energy at a given wavenumber and wave age to that predicted by the B90 relationship [Eq. (2.2)].

b. *The role of the spectral tail*

1) PRELIMINARY REMARKS ON THE COMPUTATIONAL METHODOLOGY

As the numerical method used to evaluate S_{nl} in the present model differs from that used in the study of

KHH, a series of initial runs were performed with a prescribed (or constrained) tail of the form f^{-5} for frequencies above $2.5f_p$. The runs had the standard KHH S_{in} term and the M2 dissipation defined by KHH. Wind speeds of U_{10} = 5, 10, and 20 m s^{-1} were used and the runs given the names K5CT, K10CT, and K20CT, respectively, in Table 1. Corresponding values of u_* for use in S_{in} were determined using the formulation of Wu (1982). To the accuracy with which the published results of KHH could be compared, the present model produced essentially identical results.

With the model performance established, the constrained tail was removed and explicit computations (designated UT in Table 1) were conducted for all wavenumbers within the computational grid. This procedure has a significant computational penalty with typical computation times rising by more than an order of magnitude. This occurs since much smaller space steps are required to maintain numerical stability in the rapidly responding high wavenumber regions of the spectrum. As a result, computational times for typical runs were as long as 10 days on a dedicated IBM RS6000/530 (approximately 25 Mflops) workstation. Hence, runs were terminated as soon as obvious trends were apparent. As a result, the figures presented in the remainder of this paper terminate at a variety of stages of development. In all cases, the available computational results are presented. Although runs were performed at different wind speeds, we concentrate here on the case with U_{10} = 10 m s^{-1} (K10UT of Table 1).

Although the UT run has no direct artificial constraint on the tail behavior, the computational tail extension [section 3b(1)] was used to represent the spectrum for wavenumbers beyond the last computational wavenumber (0.540 cpm) of the discrete spectral grid. This was included to account for nonlinear interactions with spectral components above this high wavenumber cutoff. In principle, this is similar to the diagnostic tail imposed in the CT run for $f > 2.5f_p$. In practice, however, the results are very different. Extensive numerical sensitivity tests showed that, provided the explicit computational grid was extended to quite high wavenumbers, such as used here, the computational tail extension only biased the highest two or three spectral wavenumber bins. These components were excluded from all subsequent analysis. In contrast, the diagnostic tail of the CT run significantly influences the development of the entire spectrum, as it is applied at wavenumbers relatively close to the energetic spectral peak.

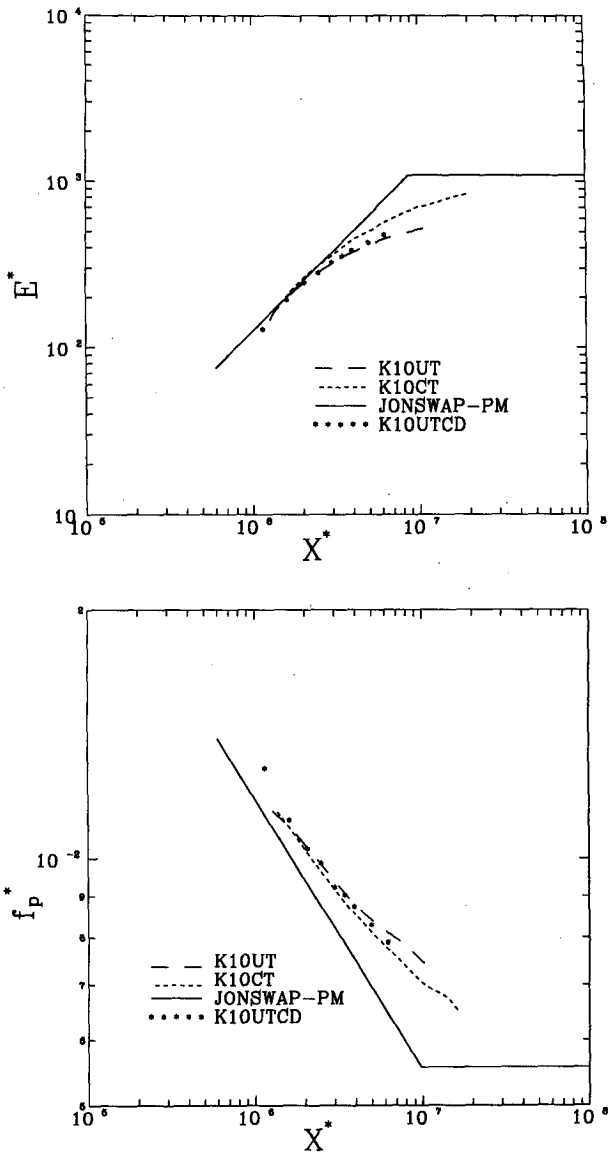

FIG. 2. Growth rates for the constrained (K10CT) and unconstrained (K10UT) tail runs compared with the JONSWAP–PM result. The results for the sea state–dependent C_d run (K10UTCD) are also shown.

2) COMPUTATIONAL RESULTS

Figure 2 shows the nondimensional growth rate and peak frequency development for runs K10CT and K10UT compared with the JONSWAP-PM results. Both runs exhibit growth rates significantly lower than the observations with a very slow transition to full development. The K10CT run, however, appears to asymptote close to the PM level. Indeed the dissipation was tuned by KHH to ensure such asymptotic large fetch behavior. The K10UT run yields significantly lower growth rates and higher values of f_p^* than either K10CT or the JONSWAP data and appears to asymptote well below the PM limit. This result is surprising as the only difference between the two runs is the removal of the constrained tail. It should be recalled that the constrained tail was originally included by KHH merely to increase computational efficiency and was claimed to have no influence on spectral development.

Figure 2 clearly shows that the tail has a marked influence, not only locally on the spectral evolution of the tail but also on the development of the energy-containing spectral region at lower wavenumbers.

Figure 3 shows values of the nondimensional spectral parameters α and n [Eq. (5.1)] as functions of wave age C_p/u_*. The B90 results are compared with both K10CT and K10UT runs. The B90 result yields an exponent n equal to -4.0. The K10CT result is also $n = -4$, as this corresponds to the selected constrained tail form [$E(f) \propto f^{-5}$]. The unconstrained tail run, K10UT, yields a high wavenumber form that decays less rapidly with a value of n approximately equal to -3.6. The values of α vary quite markedly, with K10UT being less than the B90 result and the K10CT result being larger. In addition, $\epsilon = 2.60$ for K10UT and $\epsilon = 1.68$ for K10CT. Hence, a very different structure of the high ($k > 6.25k_p$) wavenumber tail emerges for the two runs. The imposition of the constrained tail has resulted in significantly less energy in the high wavenumber regions than for the unconstrained tail case.

Clearly, the imposition of the artificial constrained tail for $f > 2.5f_p$ has had a significant influence on the development of the spectrum. Since the dissipation term was determined by KHH using a constrained tail model, relaxation of the constrained tail now yields results at considerable variance with observations. To understand why the tail should have such a significant influence requires a detailed investigation of the individual source terms.

Figure 4 shows polar-shaded isoline plots of the directional wavenumber spectrum together with each of the source terms for the two runs. The two spectra shown in Fig. 4, one with the constrained tail (Fig. 4a) and one without (Fig. 4b) were selected such that the total energy of the two spectra ($E^* \approx 4.57 \times 10^2$) were within 1% of each other. To the accuracy with which f_p (and hence C_p) can be determined in a discrete spectral model, the wave ages of the two spectra were also equivalent. Due to the different growth rates of the two cases, however, the spectra are from very different fetches. The ordinates of the directional spectra are very similar in magnitude. Both spectra have a "squarer" directional spread than could be expected for typical $\mathrm{sech}^2\beta\theta$-type directional distributions. The isolines have less curvature than the angular grid lines of the plots and hence cut the angular grid. This is an indication that more energy is located at angles to the wind than in the wind direction. This feature, which is stronger for K10CT than K10UT, will be highlighted later. The widths of the directional spreads also differ. K10CT is broader near the spectral peak and narrower in the tail.

The atmospheric input, S_{in}, and dissipation, S_{ds}, are similar both in magnitude and shape for the two runs. The minor differences are due to the slightly different

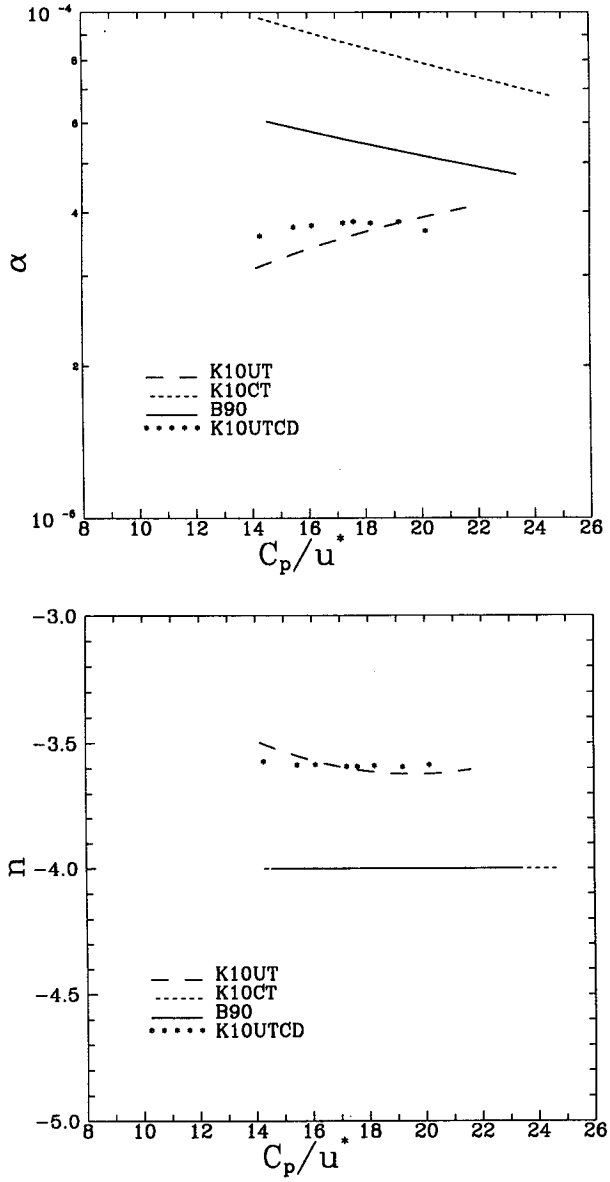

FIG. 3. Values of α and n from Eq. (5.1) as a function of wave age. Results for the runs described in Fig. 2 are presented. For comparative purposes, the Banner (1990) (B90) results are also presented.

directional spreading of the respective spectra. It is noticeable that the directional spread of S_{in} is narrower than S_{ds}. The directional dependence in S_{ds} occurs due to a product involving $F(\underline{k})$ [see Eq. (4.1)]. In contrast, S_{in} involves both a product with $F(\underline{k})$ and a cosine dependence on the angle to the wind. Hence, S_{in} decays more rapidly with direction from the wind.

The nonlinear terms, S_{nl}, for both runs show the typical plus–minus signature previously shown in one-dimensional presentations of S_{nl} (Hasselmann and Hasselmann 1981), in which energy is transferred to

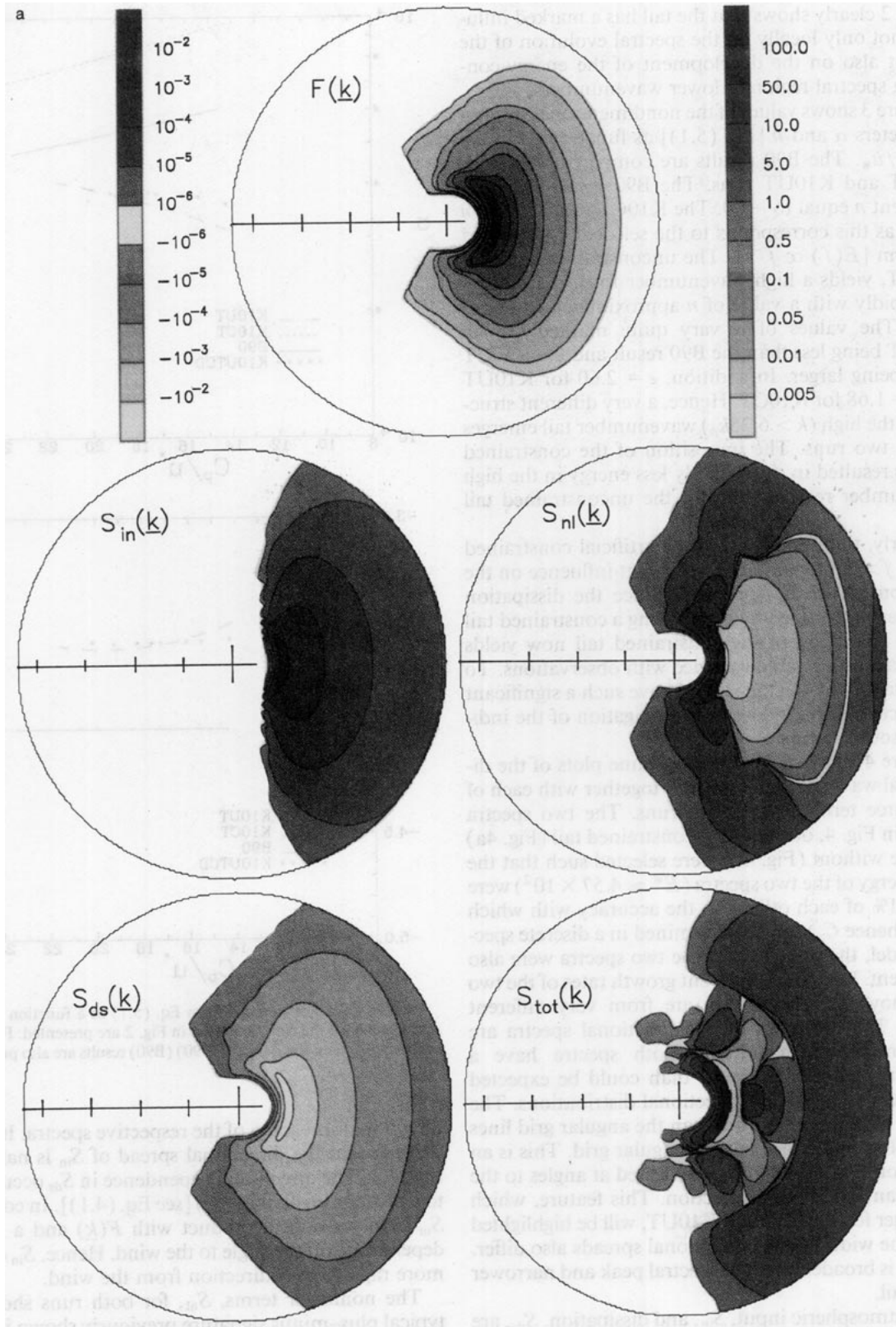

FIG. 4. Two-dimensional polar representations of the wavenumber spectrum and the three source terms, together with the total source term. Results are for (a) the constrained tail run, K10CT, and (b) the unconstrained tail run, K10UT. The color bar at the top right corresponds to the spectrum, $F(\underline{k})$ (units m^{-4}), while the coded bar to the left relates to the source term plots (units $m^4 s^{-1}$). The radial tick marks are drawn at the origin, k_p, $4k_p$, $9k_p$, and $16k_p$.

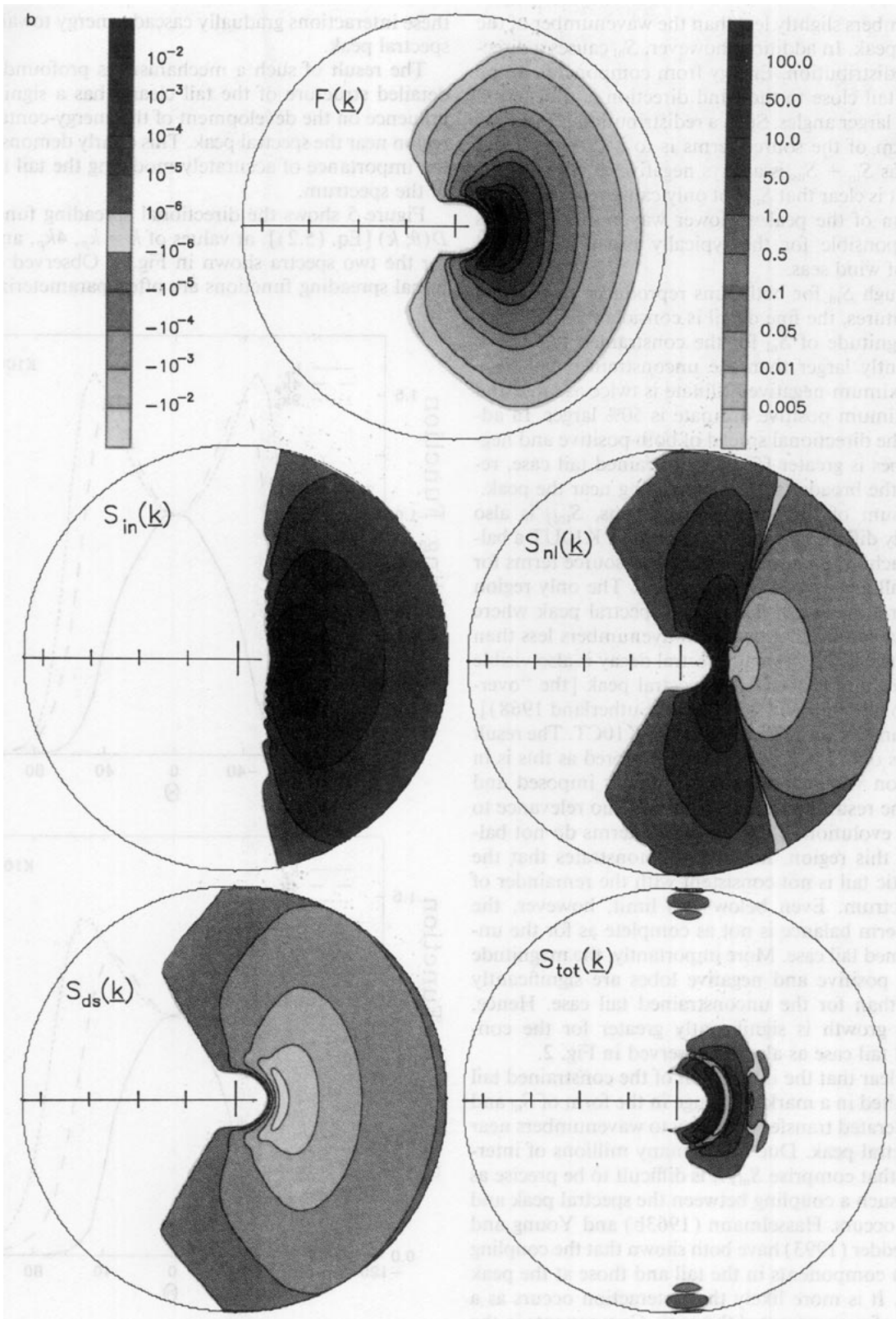

FIG. 4. (*Continued*)

wavenumbers slightly less than the wavenumber of the spectral peak. In addition, however, S_{nl} causes a directional redistribution. Energy from components in the spectral tail close to the wind direction is transferred to much larger angles. Such a redistribution is required if the sum of the source terms is to be zero in these regions as $S_{in} + S_{ds}$ is always negative at such angles. Hence, it is clear that S_{nl} not only causes the continual migration of the peak to lower wavenumbers but is also responsible for the typically broad directional spread of wind seas.

Although S_{nl} for both runs reproduces these same gross features, the fine detail is considerably different. The magnitude of S_{nl} for the constrained tail run is significantly larger than the unconstrained tail case. The maximum negative ordinate is twice as large and the maximum positive ordinate is 50% larger. In addition, the directional spread of both positive and negative lobes is greater for the constrained tail case, reflecting the broader spectral spreading near the peak.

The sum of the three source terms, S_{tot}, is also markedly different in the two cases. For K10UT a balance is achieved between the various source terms for almost all angles and wavenumbers. The only region of spectral evolution is near the spectral peak where there is a continual growth at wavenumbers less than the spectral peak. A small spectral decay is also visible at wavenumbers above the spectral peak [the "overshoot" phenomenon (Barnett and Sutherland 1968)]. The balance is far more complex for K10CT. The result at values of $k > 6.25k_p$ should be ignored as this is in the region where the diagnostic tail is imposed and hence the resulting source terms have no relevance to spectral evolution. That the source terms do not balance in this region, however, demonstrates that the diagnostic tail is not consistent with the remainder of the spectrum. Even below this limit, however, the source term balance is not as complete as for the unconstrained tail case. More importantly, the magnitude of both positive and negative lobes are significantly greater than for the unconstrained tail case. Hence, spectral growth is significantly greater for the constrained tail case as already observed in Fig. 2.

It is clear that the imposition of the constrained tail has resulted in a marked change in the form of S_{nl} and an accelerated transfer of energy to wavenumbers near the spectral peak. Due to the many millions of interactions that comprise S_{nl}, it is difficult to be precise as to how such a coupling between the spectral peak and the tail occurs. Hasselmann (1963b) and Young and Van Vledder (1993) have both shown that the coupling between components in the tail and those at the peak is weak. It is more likely that interaction occurs as a cascade of energy toward the peak. Components in the tail will interact with neighboring components at slightly lower frequencies and as the spectrum evolves these interactions gradually cascade energy toward the spectral peak.

The result of such a mechanism is profound. The detailed structure of the tail clearly has a significant influence on the development of the energy-containing region near the spectral peak. This clearly demonstrates the importance of accurately modeling the tail region of the spectrum.

Figure 5 shows the directional spreading function, $D(\theta; k)$ [Eq. (5.2)], at values of $k = k_p$, $4k_p$, and $9k_p$ for the two spectra shown in Fig. 4. Observed directional spreading functions are often parameterized in

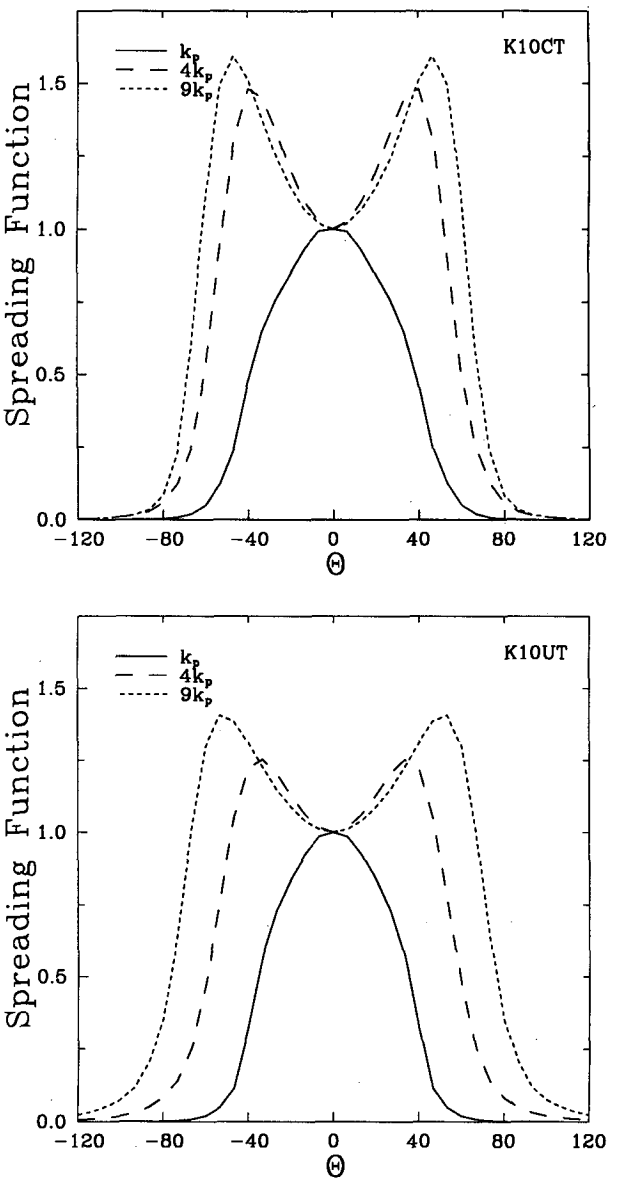

FIG. 5. Angular spreading functions as defined by Eq. (5.2) for runs K10CT and K10UT. An angle of $\theta = 0$ corresponds to the wind direction.

terms of unimodal forms such as $\cos^{2s}\theta/2$ (D. Hasselmann et al. 1980; Mitsuyasu 1975) or $\text{sech}^2\beta\theta$ (DHH). In contrast to these forms, the spreading functions shown in Fig. 5 are unimodal at the spectral peak but become bimodal at higher frequencies. More energy is contained in off-wind directions than in the wind direction. The magnitude of these side lobes is greater in the K10CT run than in the K10UT run. These features were also evident in Fig. 4.

Although spreading functions of this form appear quite strange, Fig. 4 shows that they produce plausible directional spectra. Although the bulk of observational data favors unimodal forms for the spreading function, there is some evidence for the existence of bimodal distributions in the high directional resolution data of Holthuijsen (1983), DHH, and Walsh et al. (1989). It is clear that more extensive observational studies with high directional resolution instruments are required to resolve whether such features really exist.

Again, an explanation of how such sidelobes develop requires an examination of the individual source terms. As mentioned above, the directional dependence in S_{in} occurs through a linear dependence on the directional wavenumber spectrum $F(\underline{k})$ and through a cosine dependence on the angle to the wind vector. In contrast, the only directional dependence in S_{ds} occurs through a linear dependence on $F(\underline{k})$. Hence, S_{in} must decay more rapidly with direction from the wind than S_{ds} (see Fig. 4) and thus the sidelobes cannot develop due to an imbalance between these terms. As shown in Fig. 4 and reported by Young and Van Vledder (1993), S_{nl} causes a directional broadening of the spectrum and it is evident that it is the nonlinear term that is responsible for the creation of the sidelobe structure.

This mechanism also explains why the sidelobes are larger in the K10CT run than the K10UT run, S_{nl} being of larger magnitude for K10CT. This can be seen more clearly by examining the development of the sidelobe ratio, λ [Eq. (5.3)], as a function of wave age.

Figure 6 shows $\lambda(4k_p)$ as a function of wave age for both K10CT and K10UT. The considerably larger sidelobes in the constrained tail run are clearly visible. It is also interesting to note that as the runs approach full development, the magnitude of the sidelobes decreases. This occurs since the magnitude of S_{nl} decreases as the spectrum approaches full development (Young et al. 1987; Young and Van Vledder 1993).

Figure 7 shows the development of the mean spectral width, $\bar{\theta}$ [Eq. (5.4)], as a function of wave age for K10CT, K10UT, and the B90 result. Both model results are similar and produce spectra that are broader than the observational data at the spectral peak and narrower than the observations in the spectral tail. The imposition of the constrained tail has, however, yielded spectra with a more uniform spectral width as a function of wavenumber. This occurs since the CT run has a spectral width, which is constant for $f > 2.5f_p$. The

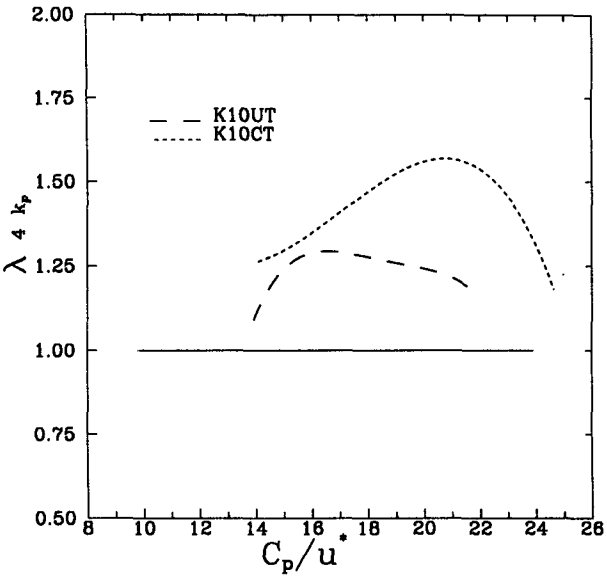

FIG. 6. The magnitude of the lobe ratio λ from Eq. (5.3) at $4k_p$ as a function of wave age. Results for runs K10UT and K10CT are shown.

interaction of this imposed fixed spectral width with the remainder of the spectrum reduces the rate of spectral broadening with wavenumber.

c. *The influence of the level of dissipation*

1) GROWTH OF WAVE ENERGY WITH FETCH

The K10CT run showed that the inclusion of the constrained tail together with the form of dissipation proposed by KHH produces growth rates consistent with observations. The details of the directional spread and high wavenumber tail are, however, not consistent with observations. Removal of the tail significantly reduces the growth rate as well as also altering the directional spread and tail structure. To obtain reasonable results with an unconstrained tail model requires a modification to S_{ds}. As an initial examination of the role S_{ds} plays in spectral development, a series of runs was performed varying the proportionality constant, c, in Eq. (4.1). Runs were performed with values of c equal to 0.1, 0.5, and 2.0 times the KHH value of 3.33×10^{-5}. These runs have been given the names K10UTN, K10UTL, and K10UTH, respectively. With the exception of the value of c, all other aspects of the runs were identical to K10UT.

Figure 8 shows the development of E^* and f_p^* as a function of nondimensional fetch. Not surprisingly, increasing the level of dissipation retards the growth rate. All runs produce growth curves that show a gradual transition to full development in a similar manner to the Lake St. Clair data and at variance with the more rapid transition in the measurements of Walsh

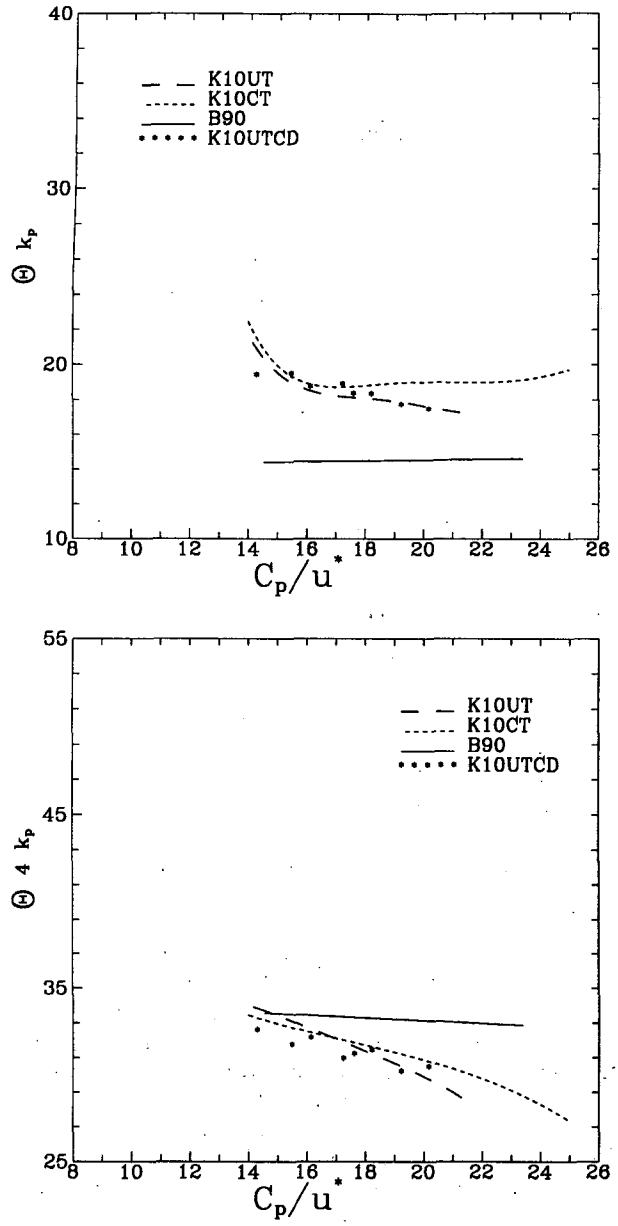

FIG. 7. The mean spectral width, $\bar{\theta}$ [Eq. (5.4)], as a function of wave age. Results are presented at k_p (top) and $4k_p$ (bottom). The results of Banner (1990) (B90) are compared with the runs K10UT, K10CT, and K10UTCD.

et al. (1989) or shown by the combined JONSWAP-PM result. At short fetches, however, the Lake St. Clair data produces growth rates that approximate a JONSWAP-type power law formulation. None of the runs in Fig. 8 reproduce this power law growth at short fetches. Run K10UTL does, however, asymptote close to the PM level. This is achieved, however, at the expense of growth rates significantly larger than the observations at shorter fetches. Thus, while there is a definite lack of agreement as to the observed form of the fetch-limited growth behavior, the computed fetch evolution for all runs departs significantly from all available data.

2) HIGH WAVENUMBER BEHAVIOR

The structure of the high wavenumber tail of the spectrum as represented by the parameters α and n is shown in Fig. 9. The level of dissipation has some influence on the exponent parameter n, which decreases with increasing dissipation. Values range between -3.3

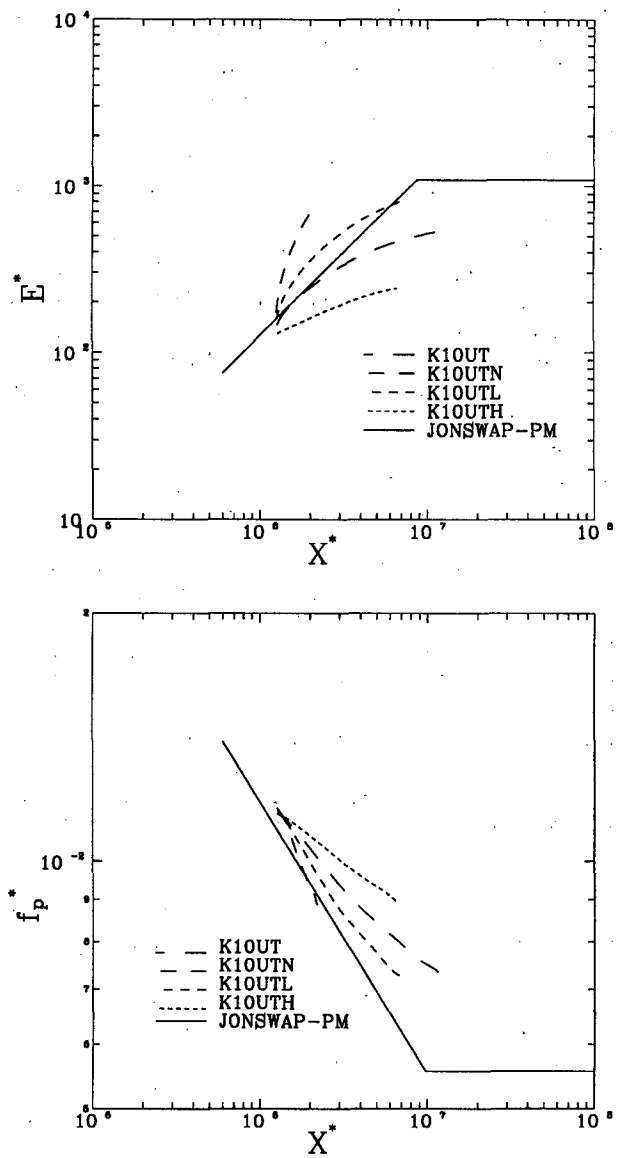

FIG. 8. Nondimensional growth rates for different values of the parameter c in the dissipation source term [Eq. (4.1)]. Results for runs K10UT, K10UTN, K10UTL, and K10UTH are compared with the combined JONSWAP–PM result.

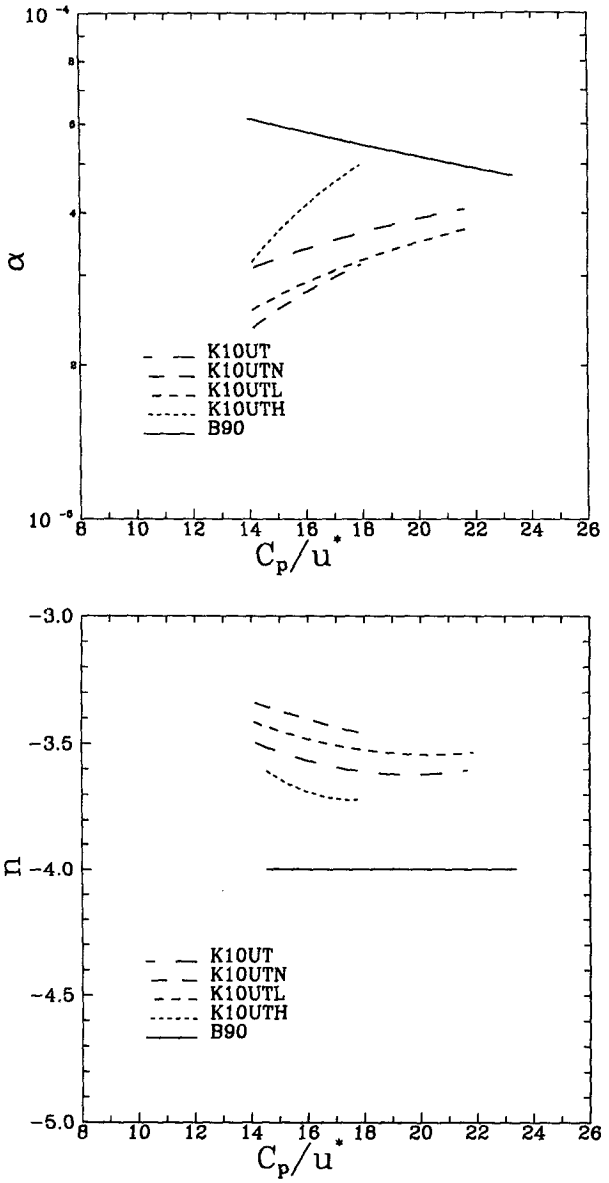

FIG. 9. Values of the parameters α and n [Eq. (5.1)] for the same runs as in Fig. 8. The results of Banner (1990) (B90) are included for comparison.

and −3.8, compared to the B90 value of −4.0. The parameter α is significantly influenced by the level of dissipation. Increasing the level of dissipation increases the value of α. In addition, all runs show that α increases as a function of wave age, in contrast to the decreasing trend reported by B90. Increasing the level of the dissipation decreases the energy in the spectral tail: for K10UTN, ϵ = 3.77; K10UTL, ϵ = 3.04; K10UT, ϵ = 2.60; K10UTH, ϵ = 2.24. Even the high dissipation run, K10UTH, however, still has significantly more energy in the spectral tail than the B90 result. Reducing the dissipation, as in the K10UTL run, produced a more favorable comparison with the observed growth rates than the original K10UT run. It has, however, resulted in a poorer reproduction of the high wavenumber ($k > 6.25k_p$) portion of the spectrum with three times the energy level proposed by B90.

3) DIRECTIONAL SPREADING

In addition to altering the high wavenumber tail structure, S_{ds} also has an influence on the directional spread. Figure 10 shows the mean width at k_p and $4k_p$ for the four cases under consideration here, together with the B90 results. At k_p all runs produce values of $\bar{\theta}$ significantly broader than those of B90. As the level of dissipation is increased, the spectral width gradually decreases. A similar situation also exists at $4k_p$ with the spectral width decreasing as the dissipation increases. All runs produce spectra that gradually broaden with increasing wavenumber, in qualitative agreement with observations. Although all runs were broader than the observations at the spectral peak, K10UT and K10UTH are narrower than the B90 result at $4k_p$.

The detailed response of the spectrum can again be explained in terms of the source term balance. Irrespective of the level of the dissipation, the spectrum always evolves to a stable equilibrium shape. This is largely due to the flexibility of the nonlinear term. An increase in S_{ds} results in an equilibrium shape with reduced energy in the spectral tail. In addition, the directional spread of the spectrum is also reduced. This occurs since it is only possible for the nonlinear terms to transfer a limited amount of energy from the mean direction to other directions. Hence, as the dissipation is increased, the sum $S_{ds} + S_{in}$ becomes negative at progressively smaller angles and the angle reduces at which the positive S_{nl} can balance these values with a nonzero spectrum.

Overall, this series of runs has clearly shown the futility of attempting to reproduce observations merely by altering the level of the dissipation. To obtain a reasonable asymptotic level, the dissipation needs to be reduced by approximately one-half as compared to K10UT. This level of dissipation, however, results in short fetch growth rates that are too high and a spectrum with far too much energy in the high wavenumber tail. In addition, the spectral width at the peak is significantly greater than reported in observations. At higher wavenumbers, the spectral width is in better agreement with observations with this level of dissipation but is still marginally too wide.

d. Distribution of dissipation within the spectrum

The above results clearly show that in order to reproduce the observed details of fetch-limited spectral

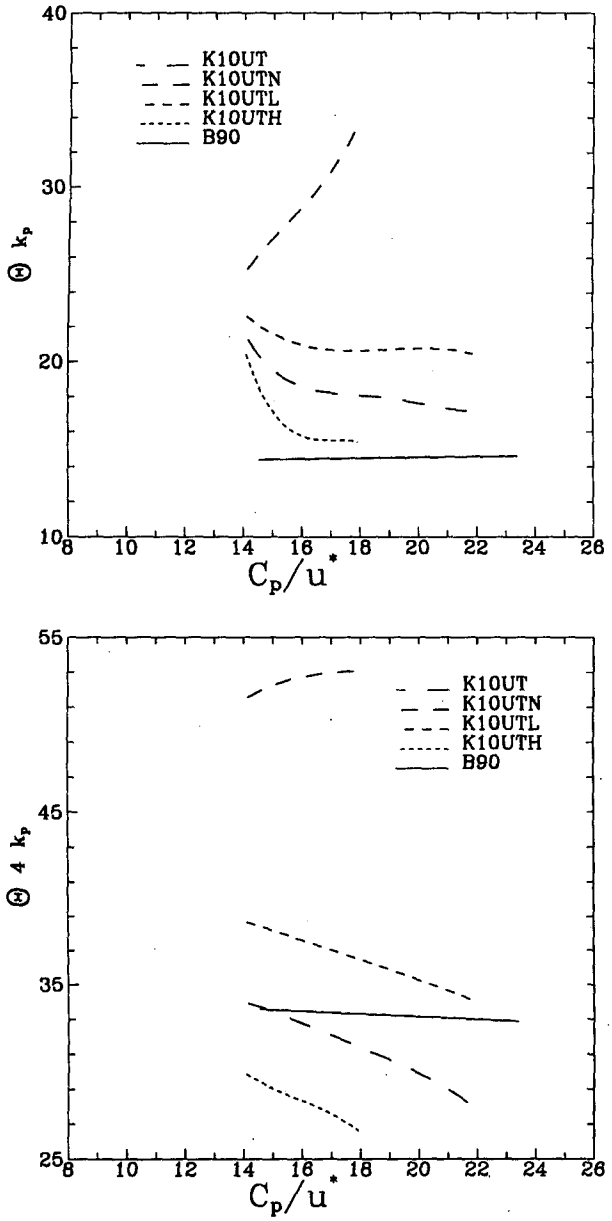

FIG. 10. The mean spectral width, $\bar{\theta}$ [Eq. (5.4)], at k_p and $4k_p$ for the same runs as in Fig. 9.

development, not only the level of spectral dissipation but also its distribution with wavenumber and direction needs to be modified. One means of altering the wavenumber distribution of S_{ds} within the framework of (4.1) is to alter the exponent l. Runs were performed with the exponent l set at 3 and 4, compared to the KHH value of 2. These runs were designated Y10UTO3 and Y10UTO4 (see Table 1). The runs are not directly comparable with K10UT as the atmospheric input term was also altered to use the Yan (1987) formulation rather than the KHH form. This alteration alone has only a minor effect on spectral development. A comparative run with the Yan (1987) input and the dissipation exponent l set at 2 was also performed, called Y10UT. This run produces similar results to K10UT. The growth rate for Y10UT is slightly lower than K10UT. This occurs since the Yan input is larger at higher wavenumbers. As a result more energy is input to the tail of the spectrum, resulting in a further elevation of the energy level in this region ($\epsilon = 3.41$ for Y10UT cf. $\epsilon = 2.60$ for K10UT). In a similar manner to the process already highlighted with the constrained tail run, the elevated tail results in a reduction in the magnitude of S_{nl}. Hence the development of the spectrum was retarded merely by a redistribution of the energy input with wavenumber. It was considered prudent to use the Yan input at this stage since a form proportional to $(u_*/C)^2$ has a greater degree of support at high wavenumbers than the KHH form. As we are now concerned with the detailed influence of dissipation on this region of the spectrum, it is essential that the most appropriate form for S_{in} is also used.

Figure 11 shows the development of both E^* and f_p^* with nondimensional fetch. Increasing the exponent l of S_{ds} in (4.1) has the effect of increasing the growth rate. Values of $l = 3$ and 4 both produce short fetch growth rates in excess of observations. A value of $l = 4$, however, appears to asymptote close to the PM level, whereas $l = 3$ falls below this level. The parameters α and n of the high wavenumber tail parameterization of the spectra are shown as a function of wave age in Fig. 12. The Y10UTO3 run produces values of α and n very similar to Y10UT. As reported for the previous cases, ϵ is greater than one ($\epsilon = 2.76$ for Y10UTO3), corresponding to a more energetic high wavenumber tail than reported by B90. A further increase in the high wavenumber dissipation as represented by the Y10UTO4 run, however, completely overpowers the other source terms and results in spectra proportional to approximately k^{-5}, high α values, and spectra with significantly reduced energy at high wavenumbers ($\epsilon = 0.96$ for Y10UTO4). Again, the mechanism by which the growth rate is altered is through S_{nl}. Increasing the dissipation at high wavenumbers results in a reduction in the level of energy in the spectral tail (as indicated by ϵ). This reduction in energy causes an increase in S_{nl} and hence accelerated growth in the spectrum.

The Y10UTO3 run produces growth rates and a wind direction slice of the wavenumber spectrum in only fair agreement with observations; the directional spread of the spectrum as shown in Fig. 13, however, is even less encouraging. Increasing the exponent l in S_{ds} results in a redistribution of the dissipation throughout the spectrum such that the dissipation is reduced near the spectral peak and increased at higher wavenumbers. This results in a broadening of the spec-

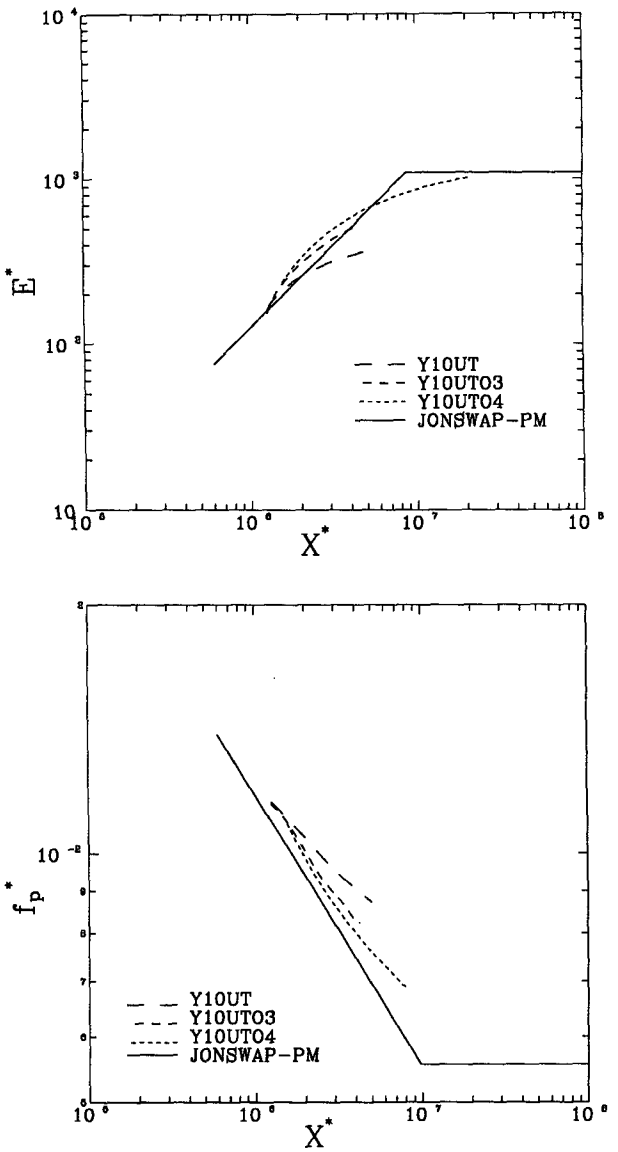

FIG. 11. Nondimensional growth rates for different values of the parameter l in the dissipation source term [Eq. (4.1)]. Results for runs Y10UT, Y10UT03, and Y10UT04 are compared with the combined JONSWAP-PM result.

trum at the peak and a narrowing at higher wavenumbers. This is the exact opposite of what was required to obtain directional spreading consistent with observations.

The sidelobe structure indicated earlier is also present in these runs as shown in Fig. 14, which presents spreading functions for three typical spectra with similar total energy and wave ages from runs Y10UT, Y10UT03, and Y10UT04. At $4k_p$ the sidelobe structure increases with an increase in the exponent l in S_{ds}. This occurs mainly since the nonlinear term that controls the development of the sidelobes increases as the energy in the spectral tail is reduced. At higher wavenumbers, however, the high levels of dissipation overcome S_{nl} and the magnitude of the sidelobes decrease. Indeed, at wavenumbers higher than those shown in Fig. 14, the directional spread returns to a unimodal form for Y10UT04.

e. *Atmospheric input*

The discussion above has focused on the sensitivity of the spectral evolution to the dissipation term S_{ds}.

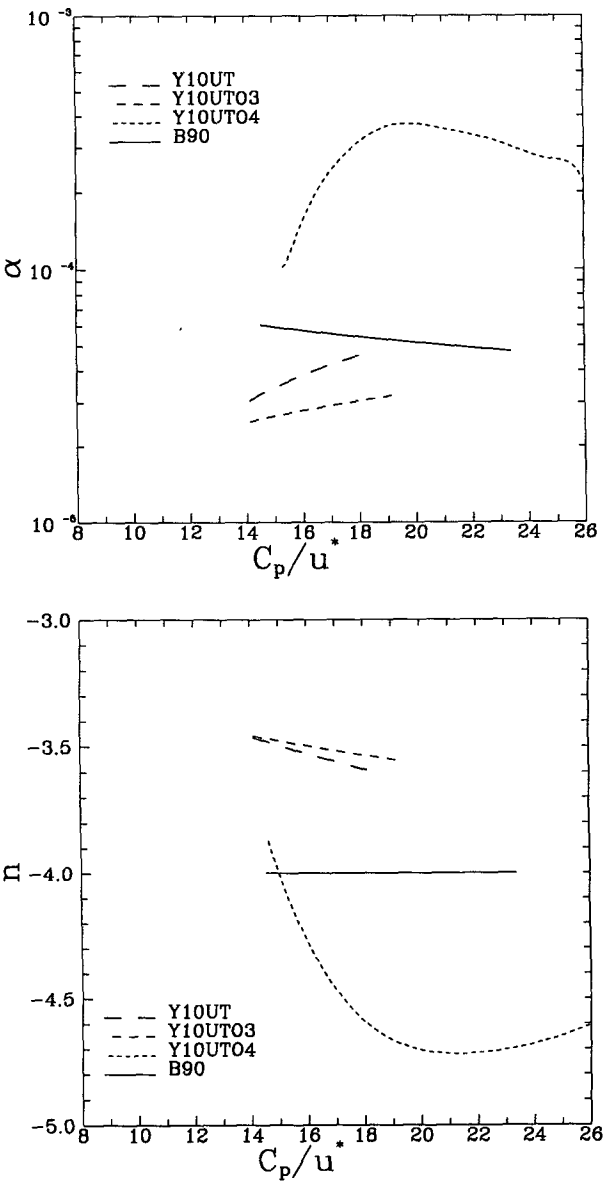

FIG. 12. Values of the parameters α and n [Eq. (5.1)] for the same runs as in Fig. 11. The results of Banner (1990) (B90) are included for comparison.

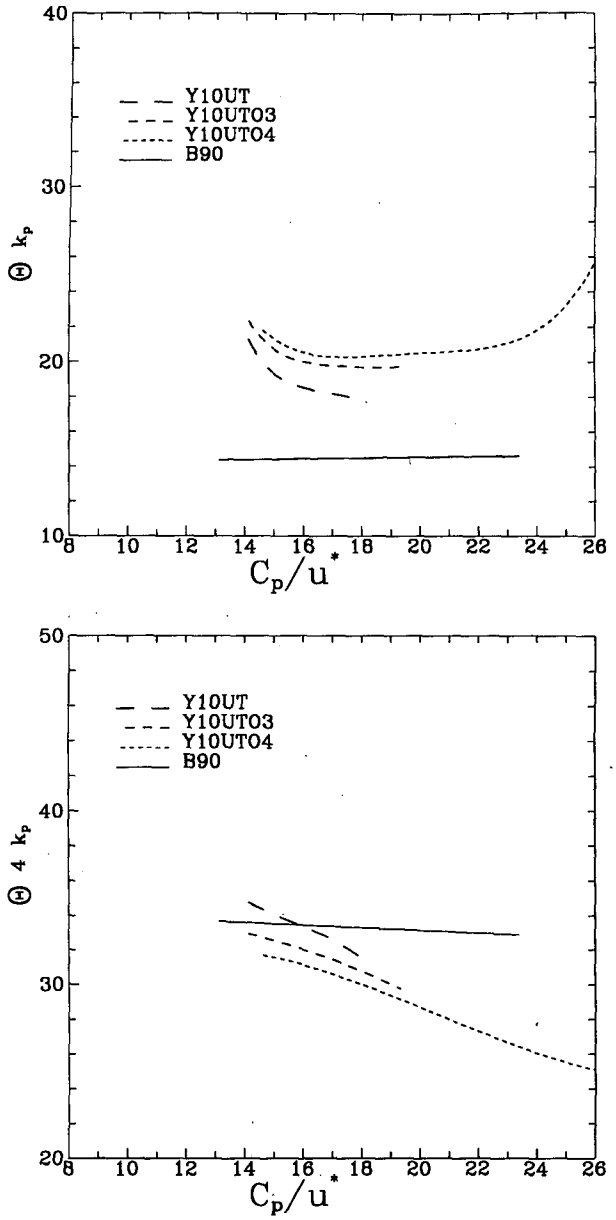

FIG. 13. The mean spectral width, $\bar{\theta}$ [Eq. (5.4)], at k_p and $4k_p$ for the same runs as in Fig. 12.

The behavior of all the diagnostics used can also be influenced by alterations in the atmospheric input term S_{in}. Whereas there is only limited theory and no measurements to support the form of S_{ds}, both theoretical formulations and comprehensive laboratory and field measurements exist for S_{in}, at least in the alongwind direction. Hence, the scope for gross errors in the formulation of S_{in} are significantly less than for S_{ds}. Debate as to the form of S_{in} has largely focused around two issues. First, whether the scaling is in terms of a characteristic wind speed parameter [U_{10}, u_* or $U(\lambda/2)$] divided by the phase speed, C, or the square of this quantity, and second, whether the drag coefficient, and hence u_*, is a function of sea state.

The consequences of introducing an S_{in} term dependent on $(u_*/C)^2$ at higher wavenumbers was investigated earlier by the introduction of the composite Yan (1987) form for the input. Although this change has an influence on spectral development, the magnitude of these changes are significantly smaller than some of the effects demonstrated with the permutations of S_{ds}.

Observations by Donelan (1982) and Geernaert et al. (1987), among others, show clearly that the aerodynamic drag coefficient, C_d, depends on the sea state. In particular, the sea surface roughness as represented by the spectral energy of the high wavenumber components of the spectrum has a significant influence on C_d. Both field data and the numerical results presented earlier clearly show that the energy in the high wavenumber portion of the spectrum, as represented by the parameters α and ϵ, is a function of wave age. Hence, it could be argued that performing fetch-limited simulations with a constant value of u_* is unrealistic. To investigate whether the apparent poor performance of the source term representations was due to the assumption of a constant value of u_*, a further simulation was performed with a constant value of U_{10}. The associated value of u_* was determined using the relationship (Geernaert et al. 1987)

$$C_d = 0.012(C_p/u_*)^{-2/3}. \tag{5.6}$$

Janssen (1989, 1991) has presented a sophisticated coupled wave–atmospheric boundary-layer analysis for the determination of the sea state dependence of C_d. As the present simulations are for fetch-limited conditions, in which the spectrum is entirely wind sea [for which simple relationships like (5.6) are valid], it was felt that the added sophistication of the full coupled analysis was not warranted.

The source terms used for this run (designated by K10UTCD) are identical to K10UT. The only difference is that u_* now varies along the fetch. When presented as a function of the nondimensional variables x^* and C_p/u_* as shown in Figs. 2, 3, and 7, the departures from the standard K10UT run for all diagnostic indicators are only minor. Hence, it appears that the sea state dependence on the aerodynamic drag has insufficient influence to account for the apparent inability of the model source terms to reproduce the observed data.

6. Conclusions

The major conclusions of this study on modeling the fetch-limited evolution of the wind wave spectrum are as follows:

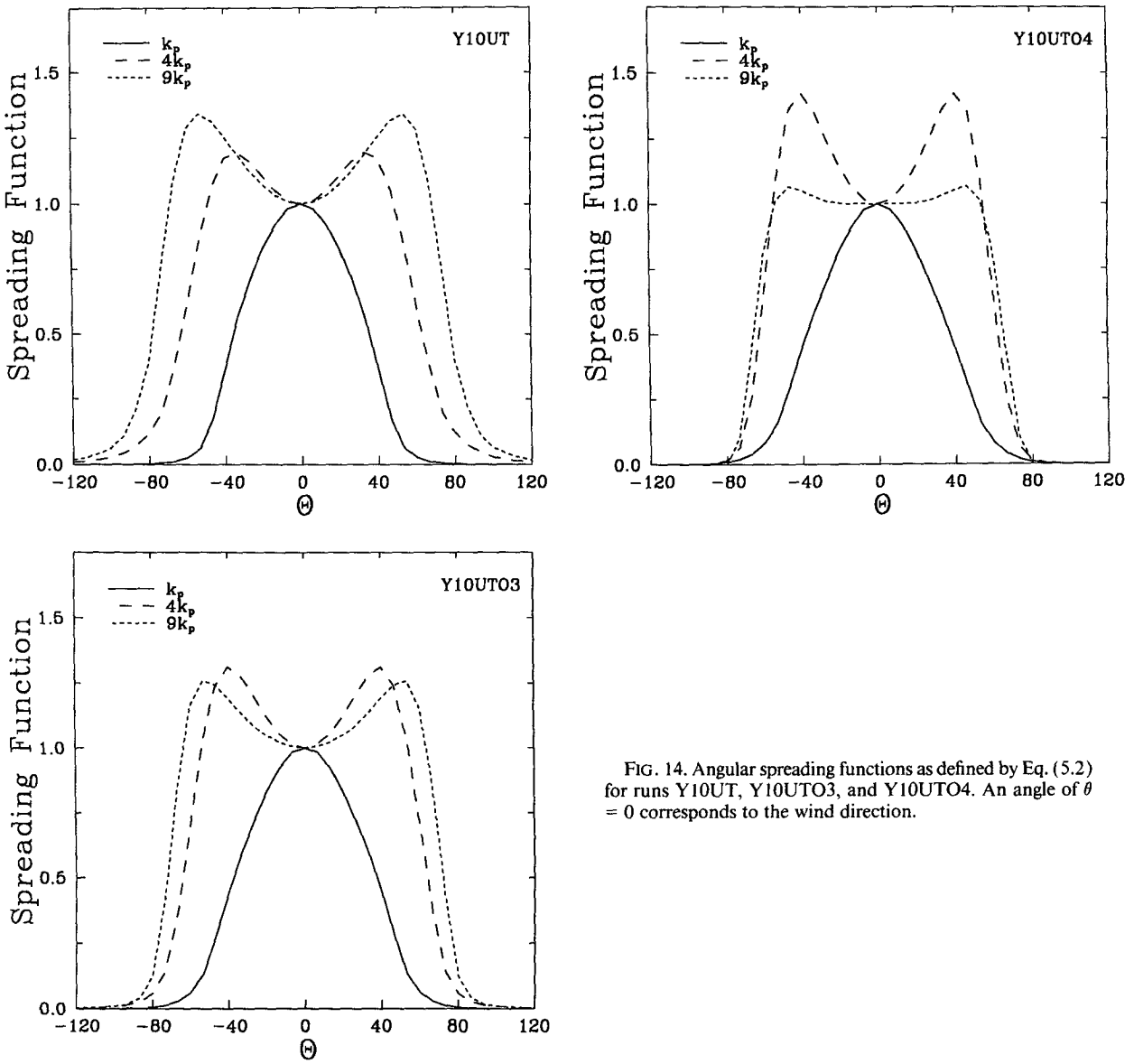

FIG. 14. Angular spreading functions as defined by Eq. (5.2) for runs Y10UT, Y10UTO3, and Y10UTO4. An angle of $\theta = 0$ corresponds to the wind direction.

1) The use of a constrained diagnostic tail shape in computational models has certain fundamental implications that were not recognized previously.

(i) The level and form of the dissipation source term $S_{ds}(\underline{k})$ required to match the observations can be very different from that required if the spectral tail shape is unconstrained and is computed as part of the model predictions.

(ii) The same $S_{ds}(\underline{k})$ applied to constrained and unconstrained tail cases can lead to very different tail shapes and to significantly different evolution of spectral energy with fetch. This interaction between the spectral tail and the energy-containing region near the spectral peak is primarily caused by $S_{nl}(\underline{k})$. These differences can be reconciled only if the form for $S_{ds}(\underline{k})$ implemented in an unconstrained tail shape calculation is intrinsically able to reproduce a spectral tail matching the prescribed constrained tail in both shape and spectral level, and even then, the directional distributions differ significantly. Therefore such constrained tail calculations may not represent realistically the balance of source terms in the spectral evolution. This is likely to provide uncertainties in the model predictions for more complex wind sea situations, such as turning winds, slanted fetches, etc., where the higher wavenumber spectrum is possibly different from the idealized fetch-limited case.

2) For unconstrained tail calculations, present variants of the Hasselmann form for $S_{ds}(\underline{k})$ do not yield a uniformly satisfactory representation for all key diagnostics: (i) the evolution of total wave energy with fetch, (ii) the directional spreading function near the spectral peak, and (iii) the form of the high wavenumber tail region. Generally the directional width at the spectral peak is broader and at high wavenumbers narrower than reported in observational data. In addition, the amount of energy in the tail is significantly higher than the observational data. Modifications to $S_{ds}(\underline{k})$ that increase the dissipation at high wavenumbers and hence reduce the energy in the tail also cause a reduction in the directional spread in this region. Hence, it is not possible to satisfy all diagnostics with the functional form of the KHH $S_{ds}(\underline{k})$ term.

3) Observed data indicates that at short fetch, the growth curve for total energy approximately follows a power law formulation (JONSWAP) and transitions smoothly to full development at larger fetches. In contrast, all variants of the source terms used here produce growth curves with no portion approximating a power law. The growth rate continually decreases with fetch. Hence, in order to obtain realistic asymptotic levels to growth, short fetch growth rates are far higher than observations.

4) For developing wave components just above the spectral peak, a very robust feature of the spectra produced by this model is the appearance of strong directional lobes that result from the nonlinear wave–wave interactions. The structure of these lobes is different for the fixed and unconstrained tail models. The existence of such characteristic directional spreading distributions remains to be confirmed in observed directional spectra, which have been limited by the poor directional resolution capabilities of pitch–roll buoys. However, recent approaches using observational techniques with superior angular resolution (e.g., DHH; Walsh et al. 1989) promise to correct this deficiency.

5) These results have potentially significant implications for third-generation operational wave models such as WAM. It is generally believed that the apparent success of WAM in predicting H_s and f_p has been due to its realistic representation of the physical source terms. The present results show that the source terms used in WAM will only produce reasonable results if the artificial diagnostic tail included in the model purely as a computational aid is retained. Even with this tail, the detailed structure of the resulting spectrum will not be consistent with observations. The inability to reproduce features such as the directional spread is likely to also influence parameters such as the directional relaxation of the spectrum under turning winds. Such effects, along with inadequate knowledge of the driving wind fields, are likely to account for the majority of the cases of poor performance of such sophisticated models.

6) Based on this study it is evident that no variation of the quasi-linear KHH form for $S_{ds}(\underline{k})$ will reproduce the detailed observational data. For the more realistic modeling of such observations, an alternate form for $S_{ds}(\underline{k})$ is required. Work toward this goal is in progress and the results will be reported in Part II of this paper.

Acknowledgments. The computer model used to perform these calculations was provided by Donald Resio of the Florida Institute of Technology. His valuable assistance in making this work possible is gratefully acknowledged. Financial support for the authors' ocean wave research by the Australian Research Council has significantly aided this study. This support is gratefully acknowledged.

REFERENCES

Banner, M. L., 1990: Equilibrium spectra of wind waves. *J. Phys. Oceanogr.*, **20**, 966–984.

——, I. S. F. Jones, and C. Trinder, 1989: Wavenumber spectra of short gravity waves. *J. Fluid Mech.*, **198**, 321–344.

Barnett, T. P., and A. J. Sutherland, 1968: A note on an overshoot effect in wind-generated waves. *J. Geophys. Res.*, **73**, 6879–6885.

Battjes, J. A., T. J. Zitman, and L. H. Holthuijsen, 1987: A reanalysis of the spectra observed in JONSWAP. *J. Phys. Oceanogr.*, **17**, 1288–1295.

Cox, C., and W. Munk, 1954: Statistics of the sea surface derived from sun glitter. *J. Mar. Res.*, **13**, 198–227.

Donelan, M. A., 1982: The dependence of the aerodynamic drag coefficient on wave parameters. *Proc. First Int. Conf. on Meteorology and Air–Sea Interactions of the Coastal Zone*, The Hague, the Netherlands, Amer. Meteor. Soc., 381–387.

——, and W. J. Pierson, 1987: Radar scattering and equilibrium ranges in wind-generated waves with application to scatterometry. *J. Geophys. Res.*, **92**, 4971–5029.

——, J. Hamilton, and W. H. Hui, 1985: Directional spectra of wind-generated waves. *Philos. Trans. Roy. Soc. London, A* **315**, 509–562.

——, M. Skafel, H. Graber, P. Liu, D. Schwab, and S. Venkatesh, 1992: On the growth rate of wind-generated waves. *Atmos.–Ocean*, **30**, 457–478.

Ebuchi, N., H. Kawamura, and Y. Toba, 1992: Growth of wind waves with fetch observed by the Geosat altimeter in the Japan Sea under winter monsoon. *J. Geophys. Res.*, **97**(C1), 809–819.

Geernaert, G. L., S. E. Larsen, and F. Hansen, 1987: Measurements of wind stress, heat flux and turbulent intensity during storm conditions over the North Sea. *J. Geophys. Res.*, **92**, 13 127–13 139.

Gelci, R., H. Cazalé, and J. Vassal, 1957: Prévision de la houle. La méthode des densités spectroangulaires. *Bull. Inform. Comité Central Oceanogr. D'Etude Côtes*, **9**, 416–435.

Hasselmann, D. E., M. Dunckel, and J. A. Ewing, 1980: Directional wave spectra observed during JONSWAP 1973. *J. Phys. Oceanogr.*, **10**, 1264–1280.

Hasselmann, K., 1960: Grundgleichungen der Seegangsvoraussage. *Schiffstechnik*, **7**, 191–195.

——, 1962: On the non-linear energy transfer in a gravity-wave spectrum. Part 1. General theory. *J. Fluid Mech.*, **12**, 481–500.

——, 1963a: On the non-linear energy transfer in a gravity-wave spectrum. Part 2. Conservation theorems; wave–particle analogy; irreversibility. *J. Fluid Mech.*, **15**, 273–281.

——, 1963b: On the non-linear energy transfer in a gravity-wave spectrum. Part 3. Evaluation of energy flux and swell–sea in-

teraction for a Neumann spectrum. *J. Fluid Mech.*, **15**, 385–398.

——, 1971: On the mass and momentum transfer between short gravity waves and larger-scale motions. *J. Fluid Mech.*, **50**, 189–205.

——, 1974: On the spectral dissipation of ocean waves due to white-capping. *Bound.-Layer Meteor.*, **6**, 107–127.

——, et al., 1973: Measurements of wind-wave growth and swell decay during the Joint North Sea Wave Project (JONSWAP). *Dtsch. Hydrogr. Z.*, **8**(Suppl. A), p. 12.

Hasselmann, S., and K. Hasselmann, 1981: A symmetrical method of computing the nonlinear transfer in a gravity wave spectrum. *Hamburger. Geophys. Einzelschr.*, **A52.**

——, ——, J. H. Allender, and T. P. Barnett, 1985: Computations and parameterizations of the nonlinear energy transfer in a gravity-wave spectrum. Part 2: Parameterizations of the nonlinear transfer for application in wave models. *J. Phys. Oceanogr.*, **15**, 1378–1391.

—— and Collaborators, 1988: The WAM Model—A third generation ocean wave prediction model. *J. Phys. Oceanogr.*, **18**, 1775–1810.

Holthuijsen, L. H., 1983: Observations of the directional distribution of ocean-wave energy in fetch-limited conditions. *J. Phys. Oceanogr.*, **13**, 191–207.

Jackson, F. C., W. T. Walton, and D. E. Hines, 1992: Sea surface mean square slope from K_u-band backscatter data. *J. Geophys. Res.*, **97**, 11 411–11 427.

Janssen, P. A. E. M., 1989: Wave-induced stress and the drag of airflow over sea waves. *J. Phys. Oceanogr.*, **19**, 745–754.

——, 1991: Quasi-linear theory of wind-wave generation applied to wave forecasting. *J. Phys. Oceanogr.*, **21**, 1631–1642.

——, P. Lionello, and L. Zambresky, 1989: On the interaction of wind and waves. *Philos. Trans. Roy. Soc. London A*, **329**, 289–301.

Kahma, K. K., and C. J. Calkoen, 1992: Reconciling discrepancies in the observed growth of wind-generated waves. *J. Phys. Oceanogr.*, **22**, 1389–1405.

Keller, W. C., and W. J. Plant, 1990: Cross sections and modulation transfer functions at L and Ku bands measured during the Tower Ocean Wave and Radar Dependence Experiment. *J. Geophys. Res.*, **95**, 16 277–16 289.

Komen, G. J., S. Hasselmann, and K. Hasselmann, 1984: On the existence of a fully developed wind-sea spectrum. *J. Phys. Oceanogr.*, **14**, 1271–1285.

Mitsuyasu, H., 1975: Observations of the directional spectrum of ocean waves using a cloverleaf buoy. *J. Phys. Oceanogr.*, **5**, 750–759.

Phillips, O. M., 1958: The equilibrium range in the spectrum of wind-generated waves. *J. Fluid Mech.*, **4**, 426–434.

——, 1985: Spectral and statistical properties of the equilibrium range in wind-generated gravity waves. *J. Fluid Mech.*, **107**, 465–485.

Pierson, W. J., and L. Moskowitz, 1964: A proposed spectral form for fully developed wind seas based on the similarity theory of S. A. Kitaigorodskii. *J. Geophys. Res.*, **69**, 5181–5190.

Plant, W. J., 1982: A relationship between wind stress and wave slope. *J. Geophys. Res.*, **87**(C3), 1961–1967.

Resio, D., and W. Perrie, 1991: A numerical study of nonlinear energy fluxes due to wave–wave interactions. Part 1: Methodology and basic results. *J. Fluid Mech.*, **223**, 609–629.

Smith, S. D., R. J. Anderson, W. A. Oost, C. Kraan, N. Maat, J. DeCosmo, K. B. Katsaros, K. L. Davidson, K. Burnke, L. Hasse, and H. Chadwick, 1992: Sea surface wind stress and drag coefficients: The HEXOS results. *Bound.-Layer Meteor.*, **60**, 109–142.

Snyder, R. L., F. W. Dobson, J. A. Elliott, and R. B. Long, 1981: Array measurements of atmospheric pressure fluctuations above surface gravity waves. *J. Fluid Mech.*, **102**, 1–59.

Toba, Y., 1973: Local balance in the air–sea boundary processes. Part III: On the spectrum of wind waves. *J. Oceanogr. Soc. Japan*, **29**, 209–220.

Tracy, B. A., and D. T. Resio, 1982: Theory and calculation of the nonlinear energy transfer between sea waves in deep water. Rep. No. 11, U.S. Army Engineer Waterways Experiment Station, Vicksburg, 47pp.

Walsh, E. J., D. W. Hancock, and D. E. Hines, 1989: An observation of the directional wave spectrum evolution from shoreline to fully developed. *J. Phys. Oceanogr.*, **19**, 670–690.

Watson, K. M., and B. J. West, 1975: A transport-equation description of nonlinear surface wave interactions. *J. Fluid Mech.*, **70**, 815–826.

Webb, D. J., 1978: Non-linear transfers between sea waves. *Deep-Sea Res.*, **25**, 279–298.

Willebrand, J., 1975: Energy transport in a nonlinear and inhomogeneous random wave field. *J. Fluid Mech.*, **70**, 113–126.

Wu, J., 1982: Wind-stress coefficients over sea surface from breeze to hurricane. *J. Geophys. Res.*, **87**, 9704–9706.

Yan, L., 1987: An improved wind input source term for third generation ocean wave modelling. Rep. No. 87-8, Royal Dutch Meteor. Inst., 20pp.

Young, I. R., and G. Ph. Van Vledder, 1993: A review of the central role of nonlinear interactions in wind-wave evolution. *Philos. Trans. Roy. Soc. London*, **342**, 505–524.

——, S. Hasselmann, and K. Hasselmann, 1987: Computations of the response of a wave spectrum to a sudden change in the wind direction. *J. Phys. Oceanogr.*, **17**, 1317–1338.